

Thermal transport in organic semiconductors

Cite as: J. Appl. Phys. 130, 170902 (2021); doi: 10.1063/5.0062074

Submitted: 1 July 2021 · Accepted: 8 October 2021 ·

Published Online: 3 November 2021



View Online



Export Citation



CrossMark

Xinyu Wang (王鑫煜),^{1,a)} Weitao Wang (王维韬),¹ Chao Yang (杨超),¹ Dan Han (韩丹),¹ Hongzhao Fan (樊弘昭),¹ and Jingchao Zhang (张景超)

AFFILIATIONS

¹ Institute of Thermal Science and Technology, Shandong University, Jinan 250061, China

² NVIDIA AI Technology Center (NVAITC), Santa Clara, California 95051, USA

a)Authors to whom correspondence should be addressed: xyw@sdu.edu.cn and jingchaoz@nvidia.com

ABSTRACT

Organic semiconductors have attracted worldwide attention and have shown great potential in emerging organic electronic devices due to their excellent properties. Advances in miniaturization and integration of organic electronic devices require understanding and tuning thermal transport capabilities of organic semiconductors to achieve desired results. In this Perspective, recent advances in the thermal transport of organic semiconductors are summarized and discussed. First, the characteristics and applications of organic semiconductors are systematically introduced. In addition, thermal conductivities of organic semiconductors and interfacial thermal conductances of different organic semiconductor-based interfaces are analyzed and summarized, respectively. Moreover, thermoelectric applications of organic semiconductors are discussed. Finally, this Perspective concludes with a summary of the current research and an outlook to guide future research in the field of organic semiconductors.

Published under an exclusive license by AIP Publishing. <https://doi.org/10.1063/5.0062074>

I. INTRODUCTION

Organic semiconductors are the most important functional components in organic electronic devices and have received tremendous attention in the past few decades owing to their great potential in various novel applications. Compared to silicon-based inorganic semiconductors, organic semiconductors have many excellent properties, including light weight, flexibility, low processing cost, and good biocompatibility, which makes organic semiconductors appropriately utilized in manufacturing flexible electronics,^{1,2} wearable devices,^{3,4} portable applications,⁵ and biomedical products.^{6,7} Particularly, the solution processability of organic semiconductors enables the mass production of organic semiconductor-driven electronics by using the printing technique, and the versatile chemical design and synthesis of organic semiconductors render vast space to modulate their optical and electrical properties, which dramatically broaden their prospects in multifunctional applications. Although several unfathomed issues still interfere with the development of organic semiconductors, immense progresses in the fabrication and characterization of organic semiconductors have transferred them from the test bench in the laboratory to industrial products and human life. Organic and inorganic semiconductors are working together to play an increasingly important and complementary role in the electronics industry.

Due to the improvement in the fabrication method of organic semiconductors and the discovery of new organic semiconductors with excellent intrinsic electrical properties, the charge mobility of organic semiconductors has been immensely boosted and reached impressive values of $20\text{--}40 \text{ cm}^2 \text{ V}^{-1} \text{ S}^{-1}$ in single crystals and hundreds of $\text{cm}^2 \text{ V}^{-1} \text{ S}^{-1}$ in ultrapure samples exceeding the charge mobility of amorphous silicon.^{8–11} The higher charge mobility of available organic semiconductors permits the increase in power of organic electronics. Nevertheless, higher power means more joule heat to be dissipated inside organic electronic devices. Different from inorganic semiconductors that can withstand high temperature of more than 100°C and still maintain considerable performance, the performance of organic semiconductors is very sensitive to temperature variation within tens of $^\circ\text{C}$. Fan *et al.* investigated the thermal stability of 2,8-bis(butyl(methyl)amino) indeno[1,2-b]fluorene-6,12-dione in α -phase and found that the relative hole mobility decreased about 60% with the temperature increasing from 25 to 70°C and even up to 90% from 25 to 100°C .¹² Organic semiconductors will spontaneously undergo morphological transformation at high temperature, resulting in the dramatic deterioration in electrical properties.^{12,13} The above phenomenon indicates that organic electronic devices require rapid heat dissipation capability to prevent heat accumulation from affecting the

device performance. However, the weak interaction between organic molecules generates poor thermal properties in organic semiconductors, which aggravates the distress of thermal transport in organic electronics.

The investigation of heat dissipation inside organic electronics is conducive to tune the heat transfer capability of organic electronics. However, the thermal transport of organic electronics is an intricate issue that deserves a comprehensive study. For instance, a number of investigations have indicated that thermal conductivities of organic semiconductors are much lower than those of inorganic semiconductors, which can be easily influenced by some factors such as the film morphology, defects, and fabrication process. Epstein *et al.* deposited pentacene on different substrates to regulate the film morphology, and experimental results demonstrated that when the size of crystalline grain decreased from 293 to 144 nm, the thermal conductivities of films diminished from 1 to $0.25 \text{ W m}^{-1} \text{ K}^{-1}$.¹⁴ In organic electronic devices, various materials, including metals, dielectrics, and organic semiconductors, are fundamentally assembled together to form layer-by-layer structures. Both carrier and phonon transports can be impeded by the multiple interfaces in layer-by-layer structures. The measured interfacial thermal conductance at the organic semiconductor–metal interface is $\sim 10 \text{ MW m}^{-2} \text{ K}^{-1}$,^{15–17} which is much smaller than those at silicon–metal interfaces.¹⁸ Notably, interfacial characteristics such as surface roughness, disorder near the interface, and interfacial interaction strength significantly affect interfacial thermal conductance, suggesting that inappropriate fabrication and assembly process may deteriorate the heat transfer capability of the interface.

In addition, organic thermoelectric materials are some specific organic semiconductors with decent thermoelectric effects, evaluated by a combination of electrical and thermal properties. Organic thermoelectric materials have inherently low thermal conductivity, which makes them superior for thermoelectric applications. In order to ulteriorly improve the thermoelectric performance of organic thermoelectric materials, the electrical properties (electrical conductivity and Seebeck coefficient) and thermal conductivity of organic thermoelectric materials should be enhanced and reduced, respectively. The demand of thermoelectric performance improvement by decreasing the thermal conductivity to a much lower level raises a different claim on tuning thermal properties for organic semiconductors, which can be realized via changing the molecular arrangement and constructing unique structures to intensify phonon scattering.

Considering the increasing power of organic electronic devices, the complexity of thermal transport within organic electronics, and the diverse needs for tuning thermal transport characteristics, thermal transport in organic semiconductor-driven devices is becoming increasingly important for future developments. In the past few decades, much attention has been paid to the investigation of thermal transport in organic semiconductors from both experimental and simulation studies. To form a comprehensive understanding of the thermal transport of organic semiconductors and lighten the prospect in future research, it is necessary to comprehensively summarize previous publications and point out research areas worth exploring in the future. This Perspective focuses on the thermal transport of organic semiconductors and summarizes the closely related progress on this topic. In Sec. II, fundamental features of organic semiconductors are

introduced first. In Secs. III and IV, experimental and simulation studies on organic semiconductors and organic semiconductor-based interfaces are summarized. In Sec. V, the thermoelectric performance of organic thermoelectric materials is discussed. Finally, the summary based on the current research and outlook guiding future developments are presented in Sec. VI.

II. CHARACTERISTICS OF ORGANIC SEMICONDUCTORS

Organic semiconductors are mainly composed of carbon, hydrogen, and some other hybrid elements. The different chemical components and internal interaction of organic semiconductors generate unique characteristics, which may essentially determine the classification, fabrication, and application of organic semiconductors. In this section, the fundamental characteristics of organic semiconductors are introduced in terms of classification, growth and characterization, and their application.

A. Classification of organic semiconductors

According to the interaction between carbon (C) atoms in organic semiconductor molecules, covalent bonds can be divided into σ bond, which cannot transport charge because of the electron localization within the bond, and π bond, which allows electrons to move freely within the molecule due to the weak bonding energy. When the corresponding π bonds in different organic molecules overlap, channels between different molecules are generated, so that charge can be transported across different organic semiconductor molecules. Meanwhile, the charge transport mechanism in organic materials is dependent on the temperature. At low temperature, the molecular vibration energy is low, and the molecules can easily form ordered crystals with each other. The carrier transport can be analyzed by a method similar to the energy band theory in inorganic semiconductors. However, at high temperature (above 150 K), charge carriers are confined in the molecule owing to violent molecular vibrations. The carrier transport among neighboring molecules takes place by hopping, which is known as the frontier orbital theory.¹⁹ In this theory, the charge transport is mainly dependent on the highest occupied molecular orbital (HOMO) and the lowest unoccupied molecular orbital (LOMO).^{20,21} Under the long-term and devotional investigation from researchers on organic semiconductors, great varieties of organic semiconductors have been excavated. In general, the two criteria for classifying organic semiconductors are based on the type of carriers and the size of molecular weight.

According to the charge carrier type, organic semiconductors can be divided into n-type (electrons as carriers), p-type (holes as carriers), and ambipolar (both holes and electrons as carriers) organic semiconductors. The carrier hopping process between molecules occurs in the HOMO or LUMO. The p-type organic semiconductors generally have a HOMO energy level of -5.0 eV ,²² which can be better matched with the commonly used electrode Au and facilitate the injection of holes. The distinguishing feature of p-type organic semiconductors is the extensive existence of benzene rings or thiophene rings in the conjugate system, which are favorable for the transport process of free electrons in π bonds, bringing about decent electrical properties. Meanwhile, some heteroatoms (such as S, N, and Se atoms) are introduced into

molecules to form hydrogen bonds for improving stability and then enhance the performance of organic materials. Currently, as a whole, the development of p-type organic semiconductors is rapid, which has exhibited decent mobility and good air stability, and significantly, some p-type organic semiconductor-based organic devices have outstanding mobilities compared with amorphous silicon devices.^{23–27} On the other hand, the electron transport in n-type semiconductors also relies on π bonds. However, the LUMO energy level of n-type organic semiconductors is mostly between -2.5 and -3.5 eV,²² which is a poor match to the work function of most metals and is not conducive to electron transfer. Therefore, the development of n-type organic semiconductors is relatively retardatory owing to inferior electric properties and poor air stability, and seeking high-performance and satisfactory-stability n-type organic semiconductors is the research hotspot for organic electronics. Ideal n-type organic semiconductors should have a lower LUMO energy level for matching the work function of metals. Otherwise, the significant injection barrier caused by mismatching will impede the process of electrons injection and transport. Introducing electron-withdrawing groups (such as halogen atoms, cyano-group, carbonyl group, and imide group) through the molecular design for modulating the molecular energy level is one of the optimal choices to improve the performance of organic semiconductors. Although some feasible strategies have been proposed to design molecular structures and enhance the performance of n-type organic semiconductors,^{28–31} it is still a demanding task to achieve a comparable performance with p-type organic semiconductors. Ambipolar organic semiconductors should possess the ability to transport both electrons and holes, which puts forward rigorous requirements on the molecular energy level. From the perspective of the energy injection barrier, ambipolar organic semiconductors should have a narrow bandgap. The constitution of the donor–acceptor system is the most promising molecule design route for obtaining solution processible high-performance ambipolar organic semiconductors.

Moreover, according to the size of molecular weight, organic semiconductors can also be classified into small molecule organic semiconductors, consisting of a single molecule within a few hundred atoms, and polymer organic semiconductors, consisting of huge numbers of reduplicative basic structural units. Small molecule and polymer semiconductors have their own specific merits and demerits in practical applications, which play irreplaceable roles in the organic electronics industry. In this Perspective, both small molecule and polymer organic semiconductors are discussed. Small molecule organic semiconductors that are mentioned in the following include pentacene, rubrene, 6,13-bis(triisopropylsilylethyanyl) pentacene (TIPS-pentacene), dinaphtho[2,3-b;2',3'-f]thieno[3,2-b]thiophene (DNTT), copper phthalocyanine (CuPc), lead phthalocyanine (PbPc), [1]benzothieno[3,2-b][1]benzothiophene (BTBT), 2,7-diethyl[1]benzothieno[3,2-b][1]benzothiophene (C8BTBT), N,N'-diphenyl-N,N'-di(3-methylphenyl)-(1,1'-biphenyl)-4,4'-diamine (TPD), and tris(8-hydroxyquinoline)aluminum (Alq₃). Polymer organic semiconductors that are mentioned in the following include poly(3-hexylthiophene) (P3HT), poly[2-methoxy-5(2'-ethyl)hexoxy-phenylenevinylene] (MEH-PPV), polypyrrole (PPy), polythiophene (PTh), poly{2,5-bis(3-tetradeethylthiophene-2-yl)thieno[3,2-b]thiophenes} (PBTBT-C14), poly[N-9'-

heptadecanyl-2,7-carbazole-alt-5,5-(4',7'-di-2-thienyl-2',1',3'-benzo-thiadiazole)] (PCDTBT), poly(3,4-ethylenedioxythiophene):tosylate (PEDOT:Tos), poly(3,4-ethylenedioxythiophene):polystyrene sulfonate (PEDOT:PSS), polyaniline (PANI), phenyl-C61-butrylic acid methyl ester (PCBM), poly{[N,N'-bis (2-octyldodecyl)-naphthalene-1,4,5,8-bis(dicarboximide)-2,6-diyl]-alt-5,5'-(2,29-bis-thiophene)} (N2200), and polythieno[3,4-b]thiophene-Tosylate (PTbT-Tos).

B. Growth and characterization of organic semiconductors

Unlike the covalent bond structure between atoms of inorganic semiconductors, the discrete molecules in organic semiconductors are confined by weak van der Waals (vdW) interaction to form bulk materials, making the performance of organic semiconductors closely related to the molecular packing, crystallinity, and growth mode. Apart from intrinsic characteristics of organic semiconductors, the growth process has a massive impact on these parameters. Organic semiconductors are usually fabricated by either vapor deposition or solution processing method. Samples prepared by different methods have different morphology features and formation processes, which will be further discussed.

In the vapor deposition method, high purity organic semiconductor powders are vaporized and then condensed into a thin film on a substrate. In the preparation process of vapor deposition, the growth mode of organic semiconductors is vital to the performance of organic devices. In general, high mobility organic semiconductor films exhibit the favorable layer-by-layer growth mode (Frank–van der Merwe mode) compared to the 3D island growth mode (Volmer–Weber mode) since the 3D island growth mode can give rise to many voids and grain boundaries in the film,^{32–34} which can impede the carrier transport and result in poor electrical properties.^{35,36} The dynamic behaviors of organic semiconductors on a substrate are mainly controlled by molecule–substrate interactions and molecule–molecule interactions. The competition between these two interactions determines the growth mode. Specifically, the stronger interaction between organic molecules and substrates will induce a greater tendency for layer-by-layer growth mode. By comparing free energies of different surfaces, the growth mode can be predicted by the following relationship:³⁷

$$\gamma_m + \gamma_i \leq \gamma_s \text{ (Frank–van der Merwe mode, layer-by-layer), } (1)$$

$$\gamma_m + \gamma_i > \gamma_s \text{ (Volmer–Weber mode, 3D island), } (2)$$

where γ_m is the surface free energy of organic semiconductors, γ_s is the surface free energy of substrate, and γ_i is the interfacial free energy. Using the work of adhesion ($w = \gamma_m + \gamma_s - \gamma_i$) to eliminate the term of γ_i , the relationship can be rewritten into the $w \geq 2\gamma_m$ for layer-by-layer mode, and $w < 2\gamma_m$ for the 3D island mode. Therefore, tuning the work of adhesion at the interface through chemical modification or self-assembled monolayers (SAMs) functionalization can directly achieve the transformation of the growth mode. Kwak *et al.* synthesized fluorinated hybrid materials to modify the work of adhesion by perfluoroalkyl chains and achieved the transformation of the growth mode from the

layer-by-layer mode to the 3D island mode.³⁸ Similarly, Wang *et al.* regulated the work of adhesion at the interface through treating dielectrics in the disparate atmosphere for different hours and achieved different growth modes of organic semiconductors [Figs. 1(a)–1(e)].³⁹ However, although this criterion has been applied to estimate the growth mode, it is essential to note that the interaction between each organic semiconductor and substrate is unique, and the consideration on the growth mode should not be totally based on the hydrophobicity and surface energy enhancement.^{35,40}

As for the solution processing method, organic semiconductors are completely dissolved by organic solvents, and then the solution is coated onto the substrate by drop-casting, spin-coating, dip-coating, or inkjet printing.^{41–43} With the evaporation of solvents, the solution changes into a supersaturated state and forms the crystal organic semiconductors. The solution processing method is considered to have great potential in manufacturing large-area array organic devices due to its simplicity and low cost. The solubility of organic semiconductors in solvents can directly affect the film quality obtained by the solution processing method. Therefore, changing the molecular structure to

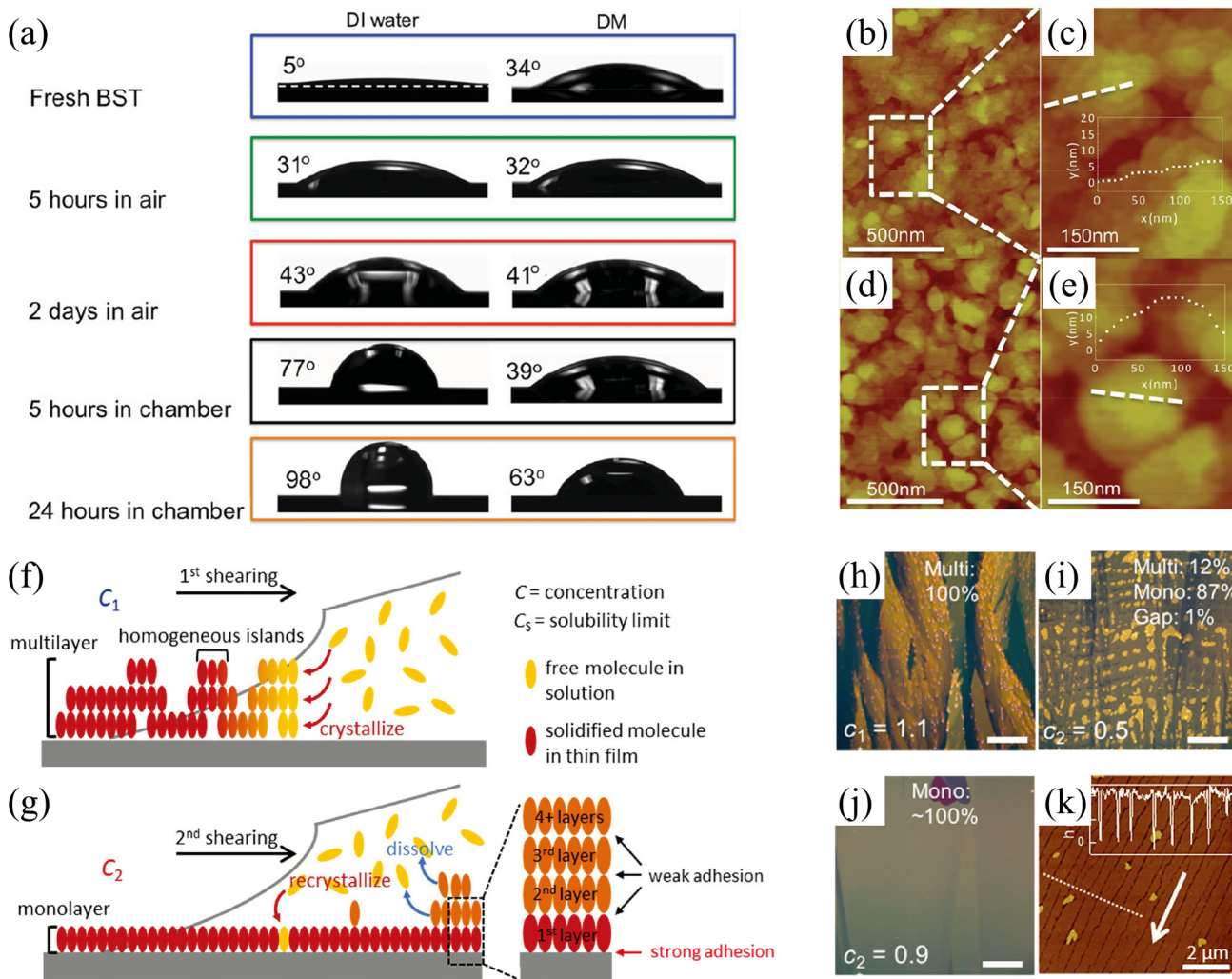


FIG. 1. (a) Contact angles of barium strontium titanate (BST) thin films under different treatments with de-ionized (DI) water and diiodomethane (DM) as probing solvent. (b) AFM image of DNTT crystals on top of 5 h stored BST. (c) The magnification image of DNTT crystal is marked in (b). The inset is the step height of DNTT layers of one crystal island. (d) AFM image of DNTT crystals on top of 24 h stored BST. (e) The magnification image of DNTT crystal is marked in (d). The inset is the step height of DNTT crystal island.³⁹ Reproduced with permission from Wang *et al.*, *Adv. Mater. Interfaces* **1**, 1300119 (2014). Copyright 2014 John Wiley & Sons. (f) and (g) Schematic illustration of the dual solution-shearing process. Dissolving (blue arrows) and recrystallization (red arrow) processes promote the growth of a highly crystallized semiconductor monolayer. (h) POM image of crystals after first shearing process. (i) and (j) POM images of crystals after second shearing processes. Scale bars: 200 μm. (k) AFM image of highly crystallized semiconductor monolayers. The white arrow denotes the shear direction. Scale bar: 2 μm. The inset is the height profile along the white dotted line.⁴⁵ Reproduced with permission from Peng *et al.*, *Adv. Funct. Mater.* **27**, 1700999 (2017). Copyright 2017 John Wiley & Sons.

improve the solubility can ameliorate the processability of organic semiconductors and thus boost the performance of organic devices. For instance, the use of siloxane-terminated solubilizing side chains in an isoindigo-based conjugated polymer could bring sufficient solubility for solution processing and decrease the intermolecular distance, which enhanced hole mobilities in thin film transistors.⁴⁴ Since complex interactions exist in the solution, including solvent–vapor interaction, solvent–substrate interaction, solute–solvent interaction, and solute–substrate interaction, it is difficult to model the growth of crystal organic semiconductors in the solution processing method, and thus most of the relevant studies are based on experiments. The solution-shearing method is one of standard methods yielding thin films for small molecule and polymer semiconductors. Specially, the dual solution-shearing method, which is modified based on the solution-shearing method, can fabricate high quality monolayer films.⁴⁵ The process of the dual solution-shearing method is schematically illustrated in Figs. 1(f) and 1(g). As shown in Fig. 1(f), after the first shearing, free molecules crystallize and form the multilayer of organic semiconductors, which can be verified by domains with different orientations and multilayer crystals observed from the polarized optical microscope (POM) in Fig. 1(h). When the second shearing is performed, the increased substrate temperature can improve the solubility of organic semiconductors, which makes crystallized molecules that weakly interact with the substrate to redissolve. By controlling the substrate temperature and semiconductor concentration, highly crystallized semiconductor monolayers are generated. The POM image of crystals after second shearing is shown in Figs. 1(i) and 1(j), which demonstrates the significance of controlling the concentration of organic semiconductor molecules. The morphology of the sample prepared by the dual solution-shearing method is assessed via the atomic force microscopy (AFM) image shown in Fig. 1(k). Aligned cracks can be observed in the AFM image, which is caused by anisotropic thermal expansion coefficients of crystal organic semiconductors and the mismatch of thermal expansion between the substrate and crystal organic semiconductors. This typical feature can also be observed by other solution processing methods.^{46,47}

C. Applications of organic semiconductors

Owing to the excellent characteristics of organic semiconductors, with the discovery of new high-performance materials and the continuous improvement of the preparation technology, organic semiconductors have been widely used to manufacture a variety of organic electronic products with different functions, which mainly include organic field-effect transistors (OFETs),^{48–50} organic light-emitting diodes (OLEDs),^{51–53} organic solar cells,^{54,55} and organic thermoelectric devices.^{56,57} Notably, although OLEDs are already in common use, other applications of organic semiconductors have not yet been commercialized. Herein, to deliver a general and basic awareness on the application of organic semiconductors, the principle, characteristics, and prospect of each type of organic electronic device are briefly introduced.

Compared with inorganic field-effect transistors, OFETs possess characteristics of low processing temperature, good compatibility with flexible polymer substrates, and suitable large-area production. Therefore, OFETs are widely used in many fields such as display devices, chem/bio-sensors, radio frequency identification

tags, large-scale integrated circuits, large-area sensor arrays, and organic lasers. In particular, OFETs have characteristics of being easy to combine with flexible substrates to realize flexible OFETs. Flexible OFETs have broad application prospects in flexible wearable devices, flexible displays, and flexible integrated circuits, which are currently among the most popular research directions in organic electronics. Meanwhile, OFETs are also developed into the direction of multifunctional OFETs acting as multifunctional devices, which usually possess novel characteristics produced by the introduction of extrinsic and intrinsic elements.⁵⁸

OLED, also known as organic electroluminescent devices, is based on the principle that organic semiconductors emit light when they are stimulated by an electric field or current. OLED-based display devices have advantages of low driving voltage, high luminous brightness, high efficiency, fast response speed, and bright colors, which can meet nowadays' requirements for better performance, greater information capacity, and more portability of display devices. In addition, OLEDs also have massive potential in lighting applications because of the low heat generation and power consumption. Significant advancements have been implemented to reach nearly 100% internal quantum efficiency. The most crucial advance in the development of OLEDs is to solve the problem of a large amount of light trapped inside the device for improving the external quantum efficiency.⁵⁹

The basic principle of organic solar cells is that after absorbing photons in organic semiconductors, electrons transfer from HOMO to LUMO to generate excitons, and charge separation occurs after the diffusion of excitons. Electrons and holes are, respectively, transferred to the cathode and anode through the action of the potential barrier to form the battery. Compared with disadvantages of the complex manufacturing process and high production cost induced by rare metals for inorganic solar cells, organic solar cells possess characteristics such as simple preparation process, low cost, and light weight, which are more suitable for promoting large-scale applications. At present, the energy conversion efficiency of organic solar cells can reach 18%,⁶⁰ which has surpassed some polycrystalline silicon solar cells. Commercial applications of organic solar cells are ushering in the dawn.

Organic thermoelectric devices are a type of vital energy devices prepared by using the thermoelectric effect of organic thermoelectric materials. Since characteristics of organic thermoelectric materials of low intrinsic thermal conductivity and excellent performance near the room temperature, organic thermoelectric materials have advantages in low-temperature power generation under tiny temperature difference and refrigeration, which have become an ideal complement to inorganic thermoelectric materials. The performance of organic thermoelectric devices has been greatly improved and rapidly developed in the past few decades. As a result, organic thermoelectric materials and devices have developed into an important field of thermoelectric materials and become a flourishing frontier of organic electronics.

III. THERMAL CONDUCTIVITY OF ORGANIC SEMICONDUCTORS

Heat carriers of organic semiconductors mainly include phonons and electrons, which can collide with others and then

produce the heat transfer phenomenon. Hence, the total thermal conductivity of an organic semiconductor is the sum of thermal conductivity contributed by phonons and electrons, i.e., $k = k_{ph} + k_e$. Nevertheless, several studies have proved that electrons have little contribution to the total thermal conductivity of undoped/lightly doped organic semiconductors.^{61–65} Thus, this section only focuses on the phonon thermal conductivity of organic semiconductors from the perspective of thermal transport theory, experimental measurement, molecular dynamics (MD) simulation, and influencing factors.

A. Thermal transport theory

For crystalline materials, the phonon thermal conductivity can be predicted by the “phonon gas model,” which is widely used to describe lattice vibrations of crystals. The phonon thermal conductivity of crystalline materials based on the kinetic theory of gas and Debye theory can be expressed as⁶⁶

$$k_{ph} = \frac{1}{3} Cv_g l = \frac{1}{3} Cv_g^2 \tau, \quad (3)$$

where k_{ph} is the phonon thermal conductivity, C is the specific heat per unit volume, v_g is the phonon group velocity, l is the phonon mean free path (MFP), and τ is the phonon relaxation time. However, unlike single crystal organic semiconductors, it is challenging to define phonon-related characteristics of amorphous organic semiconductors on account of the lack of long-range periodicity, such as phonon vibration wave vector, phonon group velocity, and phonon relaxation time. Thus, the thermal conductivity of amorphous organic semiconductors cannot be well predicted by the above “phonon gas model.” Some theoretical models on the thermal conductivity of amorphous materials have been proposed since 1992. The “minimum thermal conductivity model” has been developed by combining Einstein’s model and conclusions of Slack, which can reasonably predict thermal conductivities of many amorphous inorganic materials at high temperature.⁶⁷ Subsequently, the Allen and Feldman (AF) model has been proposed to calculate thermal conductivities of bulk amorphous materials,^{68,69} which divides the thermal conductivity into the contribution of different modes (propagons, diffusons, and locons) and perfectly explains the variation of thermal conductivities of amorphous silicon and amorphous silicon dioxide at a temperature range of 1–100 K. However, the role of anharmonicity interaction among above modes has been completely neglected in this AF model, which has a significant effect on heat transport in complex systems.⁷⁰ Hence, after considering the temperature-dependent anharmonicity, Lv and Henry introduced a new method called the “Green–Kubo modal analysis (GKMA)” and directly calculated the contribution of different modes to thermal conductivity without considering the phonon group velocity.⁷¹

Many theoretical models have been developed to estimate the thermal conductivities of crystalline materials and amorphous materials. However, compared with inorganic semiconductors composed of covalent bonds, the interactions between organic semiconductor molecules are noncovalent bonds, such as intermolecular π – π interactions, hydrogen bonds, vdW interactions, and other

weak interactions. Different interactions cause significant discrepancies in internal structures and phonon transport characteristics between inorganic and organic semiconductors. Moreover, as described above, organic semiconductors are in single crystal, polycrystalline, and amorphous structures. Therefore, current theoretical models are difficult to describe heat transport characteristics of organic semiconductors accurately. Experimental measurement and molecular dynamics simulation have been applied more widely to evaluating the thermal conductivity of the organic semiconductor.

B. Experimental measurement

Numerous experimental methods for measuring the thermal conductivity of organic semiconductor have been reported, for example, the 3- ω method, frequency-domain thermoreflectance (FDTR), time-domain thermoreflectance (TDTR), scanning thermal microscopy (SThM), membrane-based AC calorimetry, suspended micro-bridge method, Raman probing method, steady-state infrared thermography (IR), etc.^{72,73} According to the time dependence of the applied heat flow, the above experimental methods can be divided into steady-state methods and transient methods. Steady-state methods first heat the thin film samples by using current Joule heating (suspended micro-bridge method) or a light beam with selected wavelength (IR method), and then apply a constant heat flow for creating a stable temperature gradient, and finally deduce the thermal properties of organic semiconductors based on the size of the sample. Transient methods impose a time-dependent heat flow generated by laser (TDTR and FDTR methods) or alternating current (membrane-based AC calorimetry, 3- ω , and SThM methods) to thin film samples and then measure the corresponding thermal response. Subsequently, thermal properties of samples are characterized by the corresponding analytical models.

Thermal conductivities of organic semiconductors measured by experimental methods have been summarized in Table I. Intrinsic thermal conductivities of most organic semiconductors are less than $1 \text{ W m}^{-1} \text{ K}^{-1}$ near room temperature and one or two orders of magnitude lower than those of inorganic counterparts such as bulk silicon ($148 \text{ W m}^{-1} \text{ K}^{-1}$) and bulk germanium ($58 \text{ W m}^{-1} \text{ K}^{-1}$),^{109,110} which are caused by the difference between covalent bonds of inorganic semiconductors and noncovalent bonds of organic semiconductors mentioned previously. Moreover, thermal transports of organic semiconductors are anisotropic on account of the anisotropic molecular packing, which is also found in Table I. As shown in Fig. 2(a), thermal conductivities of four typical polymer organic semiconductors (P3HT, MEH-PPV, PBTTT-C14, and PEDOT:Tos) have been measured by using the membrane-based AC calorimetry and 3- ω methods. In-plane (out-of-plane) thermal conductivities of P3HT, MEH-PPV, PBTTT-C14, and PEDOT:Tos are 0.38 (0.17), 0.37 (0.19), 0.39 (0.23), and 0.86 (0.22) $\text{W m}^{-1} \text{ K}^{-1}$, illustrating the obvious anisotropic thermal transport.⁷² Thermal conductivities of PEDOT:PSS in in-plane and out-of-plane directions are 0.55 and $0.15 \text{ W m}^{-1} \text{ K}^{-1}$ deriving from anisotropic thermal diffusivities measured by the laser flash method.⁷⁷ In addition, Kim *et al.* also measured thermal conductivities of PEDOT:PSS films treated with different dopants using the 3- ω method, which were 0.42

TABLE I. Summary of thermal conductivities of organic semiconductors near room temperature.

Classification	Material	Method	Thermal conductivity (W m ⁻¹ K ⁻¹)	Direction	Reference
Polymer	PEDOT (film)	Modulated differential scanning calorimetry	0.35	In-plane	74
	PEDOT:PSS (film)	3- ω	0.22–0.32	Out-of-plane	75
			0.42–0.52	In-plane	
	PEDOT:PSS (film)	3- ω	0.15	Out-of-plane	76
			0.84	In-plane	
	PEDOT:PSS (1.7 S cm ⁻¹ , film)	Ai-phase equipment	0.15	Out-of-plane	77
		Laser flash method	0.55	In-plane	
	PEDOT:PSS (810 S cm ⁻¹ , film)	Ai-phase equipment	0.20	Out-of-plane	77
		Laser flash method	0.94	In-plane	
	PEDOT:PSS (film)	Suspended microdevice	0.50	In-plane	78
PEDOT:PSS (film)	PEDOT:PSS (film)	3- ω	0.30–0.35	In-plane	79
	PEDOT:PSS (film)	Frequency dependent photothermal measurement	0.25	Out-of-plane	80
		AC calorimetry	0.25–1	In-plane	
	PEDOT:PSS (film)	Laser flash method	0.31–0.37	Out-of-plane	81
	PEDOT:PSS (drop-cast film)	TDTR	0.3	Out-of-plane	82
	PEDOT:PSS (spin-cast film)	TDTR	0.65–1	In-plane	
			0.29	N/A	82
	PEDOT:Tos (film)	Suspended microdevice	0.7–1.8	In-plane	78
	PEDOT:Tos (film)	3- ω	0.33	Out-of-plane	83
			0.37	In-plane	
PEDOT:Tos (film)	PEDOT:Tos (film)	3- ω	0.22	Out-of-plane	72
	P3HT (film)	Membrane-based AC calorimetry	0.86	In-plane	
		Ai-phase equipment	0.21	Out-of-plane	77
		Laser flash method	0.48	In-plane	
	P3HT (film)	TDTR	0.185–0.213	Out-of-plane	84
	P3HT (film)	FDTR	0.17	Out-of-plane	85
	P3HT (film)	3- ω	0.17	Out-of-plane	72
	P3HT (film)	Membrane-based AC calorimetry	0.38	In-plane	
		3- ω	0.27	Out-of-plane	86
			0.35	In-plane	
PANI (film)	PANI (film)	Laser flash method	0.16	N/A	87
	PANI (film)	3- ω	0.04–0.14	In-plane	88
	PANI (nanowire)	Thermal conductivity analyzer (C-THERM Tech)	0.3	N/A	89
	PANI (nanorod)	Thermal conductivity analyzer (C-THERM Tech)	0.4	N/A	89
	Polythiophene (nanotube)	Photoacoustic technique	0.8–1.0	Out-of-plane	90
	PBTTT-C14 (film)	3- ω	0.23	Out-of-plane	72
		Membrane-based AC calorimetry	0.39	In-plane	
	PCBM (film)	TDTR	<0.03	Out-of-plane	91
	PCBM (film)	TDTR	0.057–0.07	Out-of-plane	92
	Polypyrrole (film)	Thermal conductivity analyzer (C-THERM Tech)	0.15–0.17	N/A	93
Polypyrrole (film)	Polypyrrole (film)	Modulated differential scanning calorimetry	0.17	In-plane	74
	Polypyrrole (film)	AC calorimetry	0.85–1.33	In-plane	94
	Polypyrrole (nanotube)	Linseis model LFA-1000	0.03–0.14	N/A	95

TABLE I. (Continued.)

Classification	Material	Method	Thermal conductivity (W m ⁻¹ K ⁻¹)	Direction	Reference
Small molecule	PCDTBT (film)	SThM	0.25	Out-of-plane	96
	N2200 (film)	3- ω	0.16	Out-of-plane	86
			0.27	In-plane	
	MEH-PPV (film)	3- ω	0.19	Out-of-plane	72
		Membrane-based AC calorimetry	0.37	In-plane	
	Pentacene (film)	3- ω	0.51	Out-of-plane	97
	Pentacene (film)	FDTR	0.27–1	Out-of-plane	14
	TPD (film)	3- ω	0.24	Out-of-plane	97
	TPD (film)	3- ω	0.11	Out-of-plane	98
			0.152–0.175	In-plane	
Small molecule	Alq ₃ (film)	3- ω	0.48	Out-of-plane	97
	DNTT (film)	3- ω	0.45	Out-of-plane	99
	DNTT (film)	3- ω	0.2	In-plane	100
	C8DNTT (film)	3- ω	0.05	In-plane	100
	CuPc (film)	3- ω	0.39	Out-of-plane	16
	CuPc (film)	TDTR	0.34	Out-of-plane	17
	CuPc (film)	SThM	0.16	Out-of-plane	101
	CuPc (film)	Frequency dependent photothermal measurement	0.4	Out-of-plane	101
	PbPc (film)	SThM	0.25	Out-of-plane	101
	PbPc (film)	Frequency dependent photothermal measurement	0.11	Out-of-plane	101
Small molecule	TIPS-pentacene (film)	3- ω	0.104	Out-of-plane	102
	TIPS-pentacene (film)	Frequency dependent photothermal measurement	0.17	Out-of-plane	103
	TIPS-pentacene (film)	AC calorimetry	1.6	In-plane	104
	BTBT (film)	SThM	0.63	Out-of-plane	63
	C8BTBT (film)	SThM	0.25	Out-of-plane	63
	Rubrene (film)	AC calorimetry	0.07	Out-of-plane	105
	Rubrene (film)	Steady-state	0.4	In-plane	106
		one-heater-two-thermometer technique			
	C ₆₀ (film)	TDTR	0.097	Out-of-plane	92
	C ₆₀ (film)	3- ω	0.16	Out-of-plane	107
Small molecule	C ₆₀ (single crystal)	Static method	0.4	N/A	108

(0.22) W m⁻¹ K⁻¹ for dimethylsulphoxide (DMSO)-mixed PEDOT:PSS film and 0.52 (0.23) W m⁻¹ K⁻¹ for ethylene glycol (EG)-mixed PEDOT:PSS film along the in-plane (out-of-plane) direction.⁷⁵

The preparation condition can impact microscopic morphologies and electrical properties of organic semiconductors. Previous studies have indicated that during the preparation of pentacene transistors, the increase of substrate temperature induces the enhancing pentacene grain size and the heterogeneous crystal structure, resulting in the increased field-effect mobility and the deteriorated bias stability.¹¹¹ Apart from electrical properties, thermal conductivities measured experimentally under different preparation conditions are also diverse. Experiments have proved that PANI prepared at room temperature presents the nanowire morphology,

while it is characterized by the nanorod morphology prepared in an ice bath.⁸⁹ PANI nanowires with smaller diameters and stronger bending and winding states suppress the phonon propagation, leading to the stronger phonon scattering and lower thermal conductivity due to the more interface hindrance. Furthermore, different preparation methods may generate different thermal transport performances of films. For eight PEDOT:Tos (S1–S7) and PEDOT:PSS (S8) samples prepared by vacuum vapor phase polymerization (VVPP) or chemical polymerization (ChP), measured thermal conductivities are shown in Fig. 2(b). It can be found that thermal conductivities of PEDOT:Tos films are extremely sensitive to preparation conditions.⁷⁸ Essentially, the effect of the preparation method on the thermal conductivity is ascribed to different microscopic morphologies of films after the preparation.

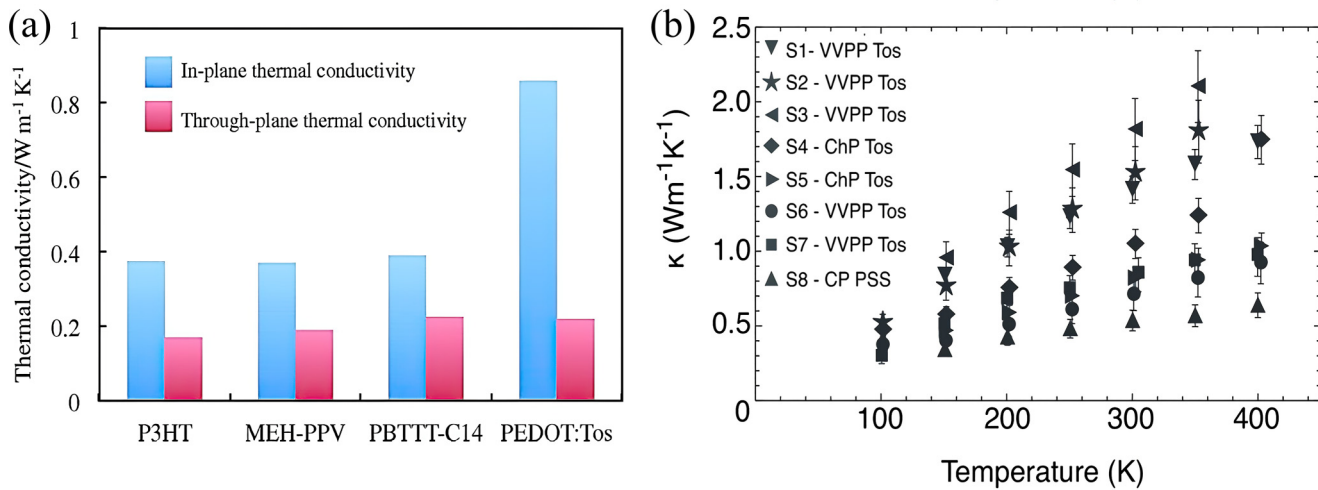


FIG. 2. (a) Anisotropic thermal conductivities of P3HT, MEH-PPV, PBTCT-C14, and PEDOT:Tos films. The through-plane in this figure represents the out-of-plane.⁷² Reproduced with permission from Ushirokita and Tada, Chem. Lett. **45**, 735–737 (2016). Copyright 2016 The Chemical Society of Japan. (b) Measured effective in-plane thermal conductivities of eight PEDOT:Tos (S1–S7) and PEDOT:PSS (S8) films prepared by VVPP or ChP. The polymerization technique is based on VVPP for S1–S3, S6, and S7, and ChP for S4 and S5. Furthermore, VVPP films S2 and S3 are prepared on different growth substrates from S1, S6, and S7.⁷⁸ Reproduced with permission from Weathers *et al.*, Adv. Mater. **27**, 2101–2106 (2015). Copyright 2015 John Wiley & Sons.

C. Molecular dynamics simulation

Except for the above experimental methods, the MD method is another powerful tool to investigate thermal conductivities of organic semiconductors in recent years. The MD method can directly solve the equation of motion of all atoms based on the classic Newton's second law, which models interactions between atoms using accurate classical force fields. In MD simulation, atoms collide with each other controlled by the force field, and positions and velocities of atoms are updated at each time step. The system behavior can be concisely described by the evolution of all atoms. Therefore, the MD method can easily extract desired thermophysical properties, such as thermal conductivity and interfacial thermal conductance. There are two typical MD methods to calculate the thermal conductivity of organic semiconductors, namely, equilibrium molecular dynamics simulation (EMD) and non-equilibrium molecular dynamics simulation (NEMD). According to the Green-Kubo formula, the EMD method obtains the thermal conductivity by calculating a time integral of the heat current autocorrelation function, which can be expressed as¹¹²

$$k_{ph} = \frac{1}{k_B T^2 V} \int_0^{\tau_0} \langle J_\alpha(0) J_\alpha(t) \rangle dt, \quad (4)$$

where k_B is Boltzmann's constant, T is the system temperature, V is the system volume, and J_α is the heat current along the α direction. For NEMD, the temperature gradient is obtained by introducing heat flux or temperature difference after the system reaches a steady state. Then the thermal conductivity is solved based on Fourier's law,

$$k_{ph} = -\frac{Q}{A \nabla T}, \quad (5)$$

where Q is the heat flux, ∇T is the temperature gradient, and A is the cross-sectional area. Thermal transport properties of organic semiconductors obtained by the MD method depend on force fields, which include many types, such as AMBER,^{113–115} OPLS,^{116,117} CHARM,^{118–120} CVFF,¹²¹ GAFF,¹²² PCFF,^{123,124} and COMPASS.^{125,126} Different force fields can be applied to describe different physicochemical properties of materials. For instance, the AMBER force field can model protein and nucleic acid condensed phase to obtain a reasonable molecular structure and configuration energy. The GAFF force field derived from the AMBER force field is more accurate for evaluating thermal properties and densities of small organic molecules. The OPLS force field is used to calculate thermal properties and solvation free energies of small organic molecules, including the united-atom force field (OPLS-UA) and the all-atomic force field (OPLS-AA). Moreover, the CHARMM force field describes small organic molecules, solutions, polymers, and other molecular systems, obtaining the reasonable structure, activation energy, and configuration energy of materials. The CVFF force field is suitable for calculating the structure and binding energy of amino acids, water, and molecular systems with different functional groups. In addition, more complex second-generation force fields, e.g., PCFF, have been developed to calculate the thermodynamic and spectral properties of molecules accurately. Afterward, based on the PCFF force field, the COMPASS force field is developed to predict the structure and cohesive energies of organic molecules, inorganic molecules, and polymers.

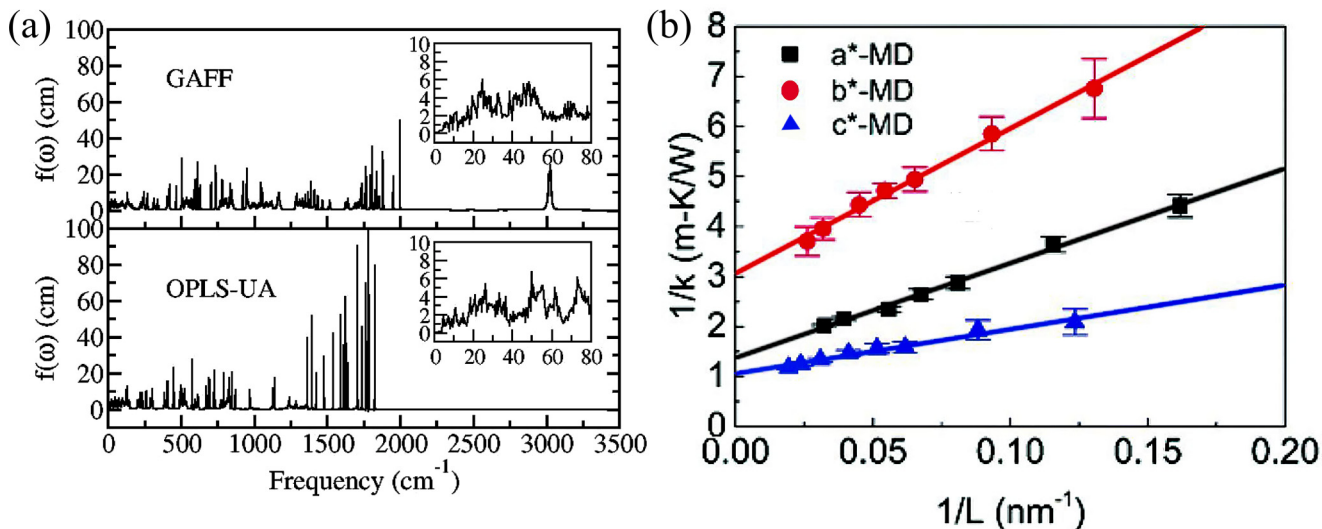


FIG. 3. (a) Phonon DOS of pentacene calculated by GAFF (upper panel) and OPLS-UA (lower panel) force fields.¹²⁷ Reproduced with permission from Wang *et al.*, J. Phys. Chem. C 115, 5940–5946 (2011). Copyright 2011 American Chemical Society. (b) Relations between $1/k$ and $1/L$ along a^* , b^* , and c^* directions of DNTT.⁶⁴ Reproduced with permission from Wang *et al.*, Nanoscale 9, 2262–2271 (2017). Copyright 2017 The Royal Society of Chemistry.

It is vital to choose applicable force fields to investigate thermal properties of organic semiconductors. Current force fields of organic materials are generally specific to one class of materials and challenging to accurately model thermal properties of a particular material. Different force fields will cause significant discrepancies in phonon behaviors, which generates different thermal properties of organic semiconductors. As shown in Fig. 3(a), Wang *et al.* used the OPLS united-atom force field and GAFF all-atomic force field to simulate the phonon density of states (DOS) of pentacene. They found that the GAFF force field could exhibit phonon vibrational properties at the high-frequency region, which was explained by the fact that the GAFF force field took into all particles in the system. In contrast, the OPLS-UA force field regarded the C atom and H atom as a united particle and removed the stretching motion of the C-H bond.¹²⁷ Moreover, thermal conductivities of PEDOT have been calculated by using PCFF and GAFF force fields. With the PCFF force field, the values in inter-chain, along-chain, and cross-plane directions are 0.2, 10, and 0.3 W m⁻¹ K⁻¹, respectively.¹¹² However, with the GAFF force field, values are 41.7 W m⁻¹ K⁻¹ in the along-chain direction and 0.3 W m⁻¹ K⁻¹ in the cross-plane direction.¹²⁸ The reason for this discrepancy is that the PCFF force field introduces higher-order terms for bond and angle, causing larger anharmonicity and lower thermal conductivity. In order to improve the accuracy of the force field, it is necessary to fit parameters based on the experimental data and quantum mechanical calculations of a specific material to obtain reasonable physical and chemical properties. Shao *et al.* successfully predicted the accurate molecular structure, crystal structure, and phonon DOS of CuPc via optimally fitting COMPASS force field parameters from both *ab initio* and empirical parametrization techniques.¹²⁹ They discovered that the predicted thermal conductivity and the experimental result still existed in discrepancy,

which was due to the difference in the preparation of simulated and experimental samples and inaccuracies in the interaction model. In recent years, with great advancements in machine learning, high-throughput computation, and the growth of materials databases, machine learning potentials (or force fields) trained with first-principles calculations or MD simulations can retain both high accuracy and general applicability to uncover the material science, which opens a promising door to calculate thermal properties of organic semiconductors.^{130–133} However, the complexity and diversity of microstructures in organic semiconductors make it challenging to consider various conditions and structural parameters of the actual preparation process in MD simulations.

Organic semiconductors are known to be susceptible to the preparation process, potentially leading to the formation of single crystals, polycrystals, and other structures. The sample size (e.g., grain size and thickness) of crystal organic semiconductors experimentally prepared is micrometers or several hundred nanometers. Meanwhile, the system dimension is limited to several tens of nanometers in NEMD simulation resulting from the restricted computational power. When the material size is smaller than or close to the phonon MFP, the phonon transport is ballistic, giving rise to the phonon-boundary scattering, which can impede the phonon thermal transport. It has been reported that phonon MFPs of typical organic semiconductors are at a range of several nanometers or tens of nanometers, which is close to the system size in NEMD simulation. Thus, thermal conductivities of organic semiconductors calculated by the NEMD method exhibit the strong size effect, which has been proved in some single crystal organic semiconductors such as pentacene,¹²⁷ DNTT,⁶⁴ BTBT,⁶³ and PEDOT.¹³⁴ To obtain the infinite length thermal conductivity, some researchers generally have combined the kinetic theory and Matthiessen's rule to fit NEMD results. Therefore, the infinite

length thermal conductivity can be extracted with the system size as follows:⁶⁴

$$\frac{1}{k_{ph}} = \frac{1}{Cv_g} \left(\frac{1}{l_{bulk}} + \frac{1}{L} \right) = \frac{1}{k_{bulk}} + \frac{1}{Cv_g} \cdot \frac{1}{L}, \quad (6)$$

where k_{bulk} is the thermal conductivity of bulk crystal material, and L is the system length. This method is widely used in many organic semiconductors to eliminate the influence of the size effect.^{64,127,128,134} Infinite length thermal conductivities of DNTT [Fig. 3(b)] and pentacene are predicted by using the NEMD method, which are 0.73 and 0.72, 0.33 and 1.1, and 0.95 and 0.61 W m⁻¹ K⁻¹ in a^* , b^* , and c^* directions, respectively.^{64,127} Moreover, calculated values of BTBT and C8BTBT are 0.95 and 0.46 W m⁻¹ K⁻¹ under the framework of isotropic approximation, respectively.⁶³ However, these infinite length thermal conductivities obtained from the NEMD method are higher than the corresponding values measured by experiment in the c^* direction (DNTT: 0.45 ± 0.06 W m⁻¹ K⁻¹, pentacene: 0.51 W m⁻¹ K⁻¹, BTBT: 0.63 ± 0.12 W m⁻¹ K⁻¹, and C8BTBT: 0.25 ± 0.13 W m⁻¹ K⁻¹).^{63,97,99} This thermal conductivity discrepancy can be attributed to two aspects: on the one hand, unlike the MD simulation, experimentally fabricated crystal organic semiconductor films generally have some defects, such as vacancy, isotope substitution, doped impurity, and grain boundary, which will enhance the phonon scattering and decrease the thermal conductivity. On the other hand, organic semiconductors, especially polymers, usually possess disordered and inhomogeneous structures, chain bending, and chain entanglement, which will reduce the phonon MFP and suppress the phonon thermal transport.

D. Influencing factors of thermal conductivity

As shown above, phonons, as the dominant heat carrier of organic semiconductors, are involved in the scattering process during thermal transport. Typical phonon scattering includes phonon-boundary scattering, phonon-phonon scattering, phonon-defect scattering, etc.¹³⁵ According to Matthiessen's rule, the total phonon relaxation time (τ_{total}) can be expressed as

$$\frac{1}{\tau_{total}} = \frac{1}{\tau_{boundary}} + \frac{1}{\tau_{ph-ph}} + \frac{1}{\tau_{defect}} + \dots, \quad (7)$$

where $\tau_{boundary}$, τ_{ph-ph} and τ_{defect} are phonon-boundary relaxation time, phonon-phonon relaxation time, and phonon-defect relaxation time, respectively. Many factors such as size, temperature, vacancy, and molecular chain, can affect phonon scattering and further modify the thermal conductivity, which is caused by the weak interaction among organic semiconductor molecules.

At the nanoscale, owing to the phonon-boundary scattering, the obvious size-dependent thermal conductivity of organic semiconductor has been described in MD simulation, which has also been demonstrated by experimental studies. The grain size of pentacene can be manipulated by depositing pentacene on different SAM-modified silicon substrates, as shown in Fig. 4(a). Epstein *et al.* investigated the effect of grain size on the thermal conductivities of pentacene films by employing the FDTR method.¹⁴ The size

of the grain formed by the growth of organic semiconductor films could directly affect the roughness of the film surface. The larger grain size generated the higher thermal conductivity of pentacene film, which resulted from the larger phonon MFP and the weakened phonon-boundary scattering [Fig. 4(b)].

According to theoretical studies of Debye and Peierls, the temperature is a significant factor in changing the phonon-phonon scattering.¹³⁵ It has been proved that the enhancing temperature can increase the phonon Umklapp scattering of organic semiconductors, reducing the phonon lifetime and phonon MFP, which causes a decrease in thermal conductivity. Both calculated thermal conductivities of DNTT⁶⁴ and PEDOT¹²⁸ exhibit a downward trend as the temperature increases, and the similar trend is also demonstrated in Alq₃.⁹⁷ For PEDOT, further investigation reveals that when the temperature increases from 200 to 300 K, the phonon MFP of PEDOT decreased by more than one order of magnitude [Fig. 4(c)], which results in the lower thermal conductivity.¹²⁸

Structural defects of organic semiconductors are inevitable during the practical preparation, introducing extra phonon-defect scattering and dominating phonon transport properties at low temperature. The most common defects are vacancies and grain boundaries. It has been proved that thermal conductivities of organic semiconductors decline with the increasing vacancy concentration. As shown in Fig. 5(a), for DNTT with a 6% vacancy concentration, reduction ratios of thermal conductivities in the a^* , b^* , and c^* directions are 44%, 33%, and 35%, respectively.⁶⁴ Analogously, for pentacene, the thermal conductivity reduces by 35% at a 4% vacancy concentration in the a^* direction.¹²⁷ The reflection, diffraction, and refraction behaviors of phonon will occur around the vacancy, which suppresses the phonon propagation because of the enhancing phonon-defect scattering and the shorter phonon MFP. Moreover, as another defect, a grain boundary is generated by different crystal orientations in polycrystalline organic semiconductors, causing the phonon-boundary scattering and the pronounced phonon localization effect, which inhibits phonon thermal transport and reduces the thermal conductivity of the organic semiconductor.¹³⁶ For example, the effects of three representative grain boundary interfaces (a^*-b^* , a^*-c^* , and b^*-c^*) on the thermal conductivity of the DNTT film have been investigated as displayed in Fig. 5(b). As the number of grain boundary interfaces increases, the thermal conductivity of DNTT decreases monotonically. For a^*-c^* and b^*-c^* interfaces, maximal reduction ratios of thermal conductivity can reach ~75%.⁶⁴

As we have already mentioned, organic semiconductor molecules are coupled with others by the weak vdW interaction, affecting the number of carrier transport channels and the carrier mobility, which impacts the electrical performance of organic semiconductors.^{137–139} Similar to electrical properties, thermal properties of organic semiconductors are also manipulated by the vdW interaction. Pressure can directly enhance the interaction between organic semiconductor molecules on account of the compressed molecule gap. It has been revealed from Figs. 6(a) and 6(b) that for organic semiconductor TPD, the increasing pressure causes the blueshift of the peak frequency of vibrational density of states (VDOS) and the larger interaction strength, which can lead to the higher phonon group velocity and thermal conductivity.¹⁴⁰

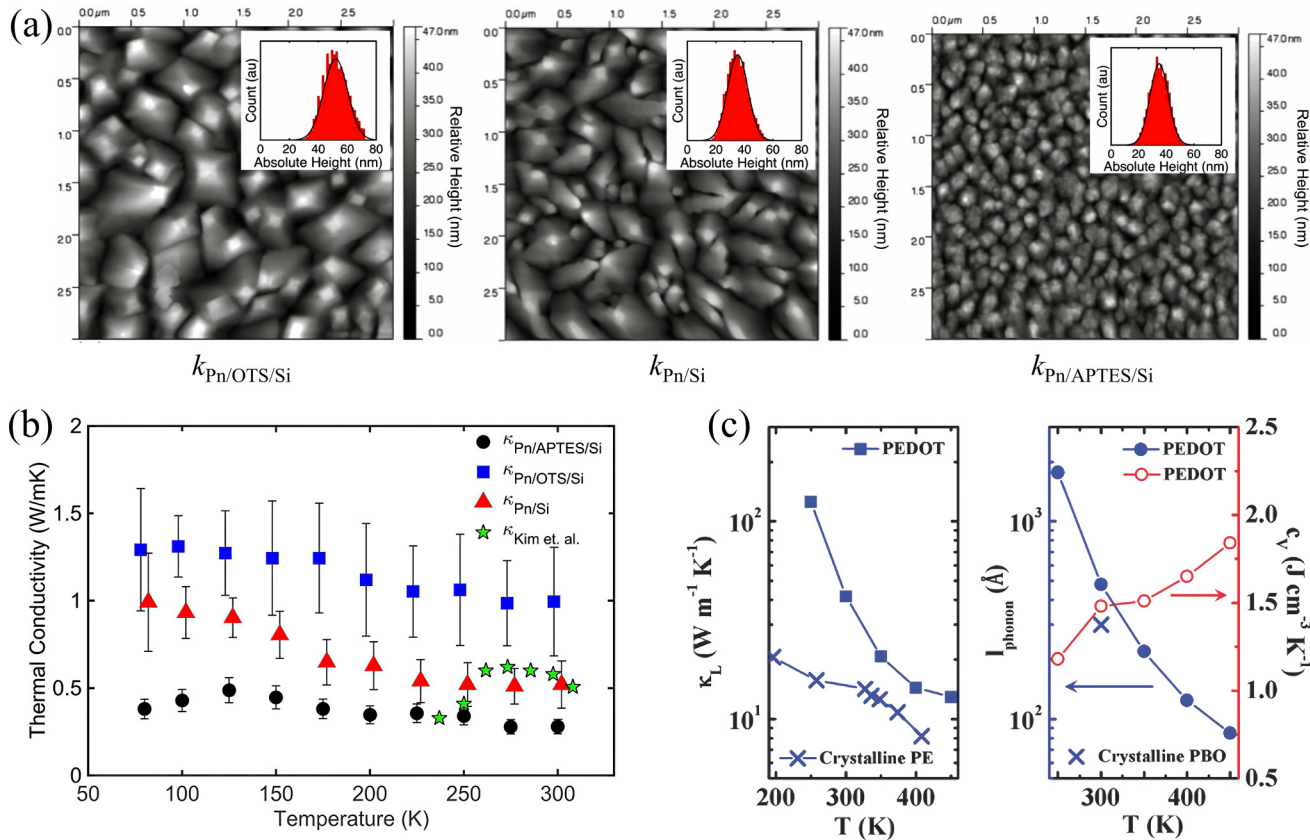


FIG. 4. (a) High resolution AFM images of relative height for pentacene (Pn) films on silicon substrates modified with SAMs composed of octadecyltrichlorosilane (OTS) and (3-aminopropyl)triethoxysilane (APTES). (b) Temperature-dependent intrinsic thermal conductivities of Pn/OTS/Si, Pn/Si, and Pn/APTES/Si.¹⁴ Reproduced with permission from Epstein *et al.*, ACS Appl. Mater. Interfaces **8**, 19168–19174 (2016). Copyright 2016 American Chemical Society. (c) Temperature-dependent axial lattice thermal conductivity and phonon MFP of PEDOT.²⁸ Reproduced with permission from Shi *et al.*, Adv. Funct. Mater. **27**, 1702847 (2017). Copyright 2017 John Wiley & Sons.

Additionally, introducing the π bond (i.e., forming the $\pi-\pi$ stacking) is another strategy to change the interaction of organic semiconductor and suppress the disorder and deformation of the molecular chain. Xu *et al.* experimentally proved that the strong $\pi-\pi$ stacking interaction of organic semiconductor P3HT films has been produced by the oxidation vapor deposition method at the deposition temperature of 318 K. The corresponding thermal conductivity was $2.2 \text{ W m}^{-1} \text{ K}^{-1}$, which was ten times larger than ordinary polymers prepared at 358 K.¹⁴¹

The configuration and arrangement of the molecular chain play a significant role in the heat transport of organic semiconductors from the above analysis, which is mainly divided into the intrinsic main chain and the introduced side chain. For polymer organic semiconductors, the amount of polymeric monomers on the main chain affects the molecular weight, and a larger molecular weight means a longer chain length, which induces a larger phonon MFP along the chain. Shi *et al.* investigated the thermal conductivities of PEDOT with different molecular weights at the similar crystallinity by MD and phonons of PEDOT with low molecular weight hindered thermal propagation due to the

localization caused by low MFP.¹²⁸ Furthermore, the disordered main chains are usually twisted and tangled together, which enhance the phonon scattering and weaken the heat transport performance. Recently, it has been reported that the alignment of the main chain can improve the regioregularity, which further reduces phonon scattering and enlarges phonon MFP. The PEDOT:PSS fiber manufactured by a continuous wet-spinning process has enhanced the regioregularity via stretching to align the main chain with the fiber axial direction, and the thermal conductivity was increased to $4\text{--}5 \text{ W m}^{-1} \text{ K}^{-1}$ at liquid nitrogen temperature.¹⁴² As shown in Figs. 6(c) and 6(d), the chain alignment of P3HT nanotubes has been achieved by a solution-based nanoporous template wetting technique, and array heights of nanotubes increase with the lengthening of the template etching time, in which the thermal conductivity is increased by fivefold compared with the bulk P3HT film.¹⁴³ Moreover, the side chain will change the main chain structure and the energy mode distribution of organic semiconductors. For the polymer organic semiconductor, polythiophene, the long alkyl side chain can increase the degree of chain distortion and result in more overlap of the molecular chain, which reduces the

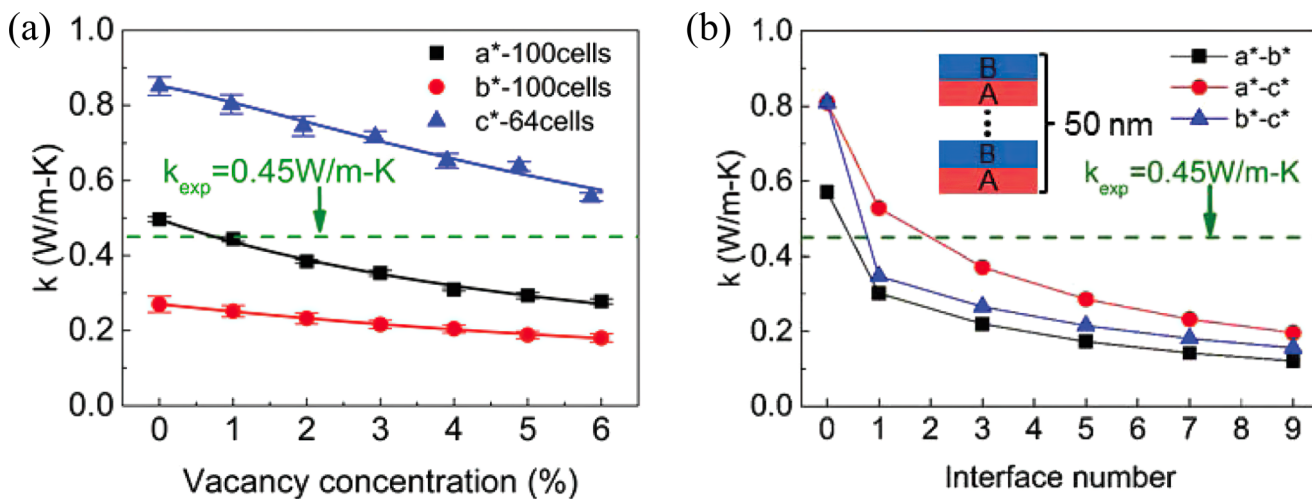


FIG. 5. (a) Thermal conductivity of DNTT in a^* , b^* , and c^* directions as a function of vacancy concentration ranging from 0% to 6% at 300 K. The green dashed line is the experimental thermal conductivity value ($0.45 \text{ W m}^{-1} \text{ K}^{-1}$). (b) Thermal conductivity of the DNTT thin film as a function of the number of grain boundary interfaces at 300 K. The total thickness of the DNTT thin film is 50 nm. Assumption that the thin film is composed of two types of crystal orientations ("A" and "B"). "A" and "B" represent a^* , b^* , or c^* crystal orientation.⁶⁴ Reproduced with permission from Wang *et al.*, *Nanoscale* **9**, 2262–2271 (2017). Copyright 2017 The Royal Society of Chemistry.

rigidity of the main chains. Moreover, introducing alkane side chains can enhance the phonon scattering and localize vibration modes of the small molecule organic semiconductor BTBT. These factors finally generate the lower thermal conductivity of polythiophene and BTBT.^{63,144,145} However, a side chain with better rigidity will increase the thermal conductivity of the organic semiconductor. For instance, organic semiconductor TIPS-pentacene with a silyl-containing side group can decrease the distribution of low-energy modes and elevate the thermal conductivity along the in-plane direction.¹⁰⁴

IV. INTERFACIAL THERMAL CONDUCTANCE OF ORGANIC SEMICONDUCTORS

The interfacial thermal conductance between different materials is another crucial factor in the nanoscale heat transfer field. The thermal transport across the interface of two materials can be affected by the phonon-boundary scattering, leading to the phenomenon that the energy carried by phonons cannot be completely transported from one side to the other at the interface, which generates the interfacial thermal resistance (ITR). This section will discuss the interfacial thermal conductance of organic semiconductor-based interfaces from the aspects of theoretical models, organic semiconductor-graphene interface, organic semiconductor–metal interface, and organic semiconductor–nonmetal interface.

A. Theoretical models of interfacial thermal conductance

The interfacial thermal transport phenomenon was first discovered at the interface between copper and liquid helium by Kapitza in 1941, which was described as the discontinuous temperature drop and subsequently proved by a large number of

experiments.^{15,63,146–149} The resistance generated by this discontinuous temperature drop is known as ITR or thermal boundary resistance (TBR), which can also be defined as the reciprocal of interfacial thermal conductance (ITC) or thermal boundary conductance (TBC). TBR is given by

$$TBR = \frac{1}{ITC} = \frac{\Delta T A_{interface}}{Q}, \quad (8)$$

where ΔT is the temperature drop at the interface, Q is the total heat flux across the interface, and $A_{interface}$ is the cross-sectional area of the interface. To predict the TBR, previous studies have proposed many models, in which the most classical theoretical models are the acoustic mismatch model (AMM) and the diffuse mismatch model (DMM). According to Snell's law, AMM assumes that the interface is a perfectly smooth plane and phonon behaviors at the interface belong to specular reflection without considering the phonon-boundary scattering. Thus, the AMM is only applicable to low-temperature or low-frequency phonon. The scattering-mediated acoustic mismatch model (SMAMM) derived from AMM has been proposed to predict TBR at high and low temperatures more accurately.¹⁵⁰ However, this model assumes that phonon transport is coherent without considering the role of inelastic phonon scattering. Contrary to AMM, DMM is used in more realistic interfaces, considering the elastic phonon scattering at the interface by randomly initializing the scattering direction and polarization, which leads to the constant TBR value when the temperature is higher than the Debye temperature. Although TBR values are predicted more accurately by this model at high temperature, many researchers still believe that not all phonons are involved in this random scattering process. Some previous MD simulations have reported that the TBR decreases linearly with the

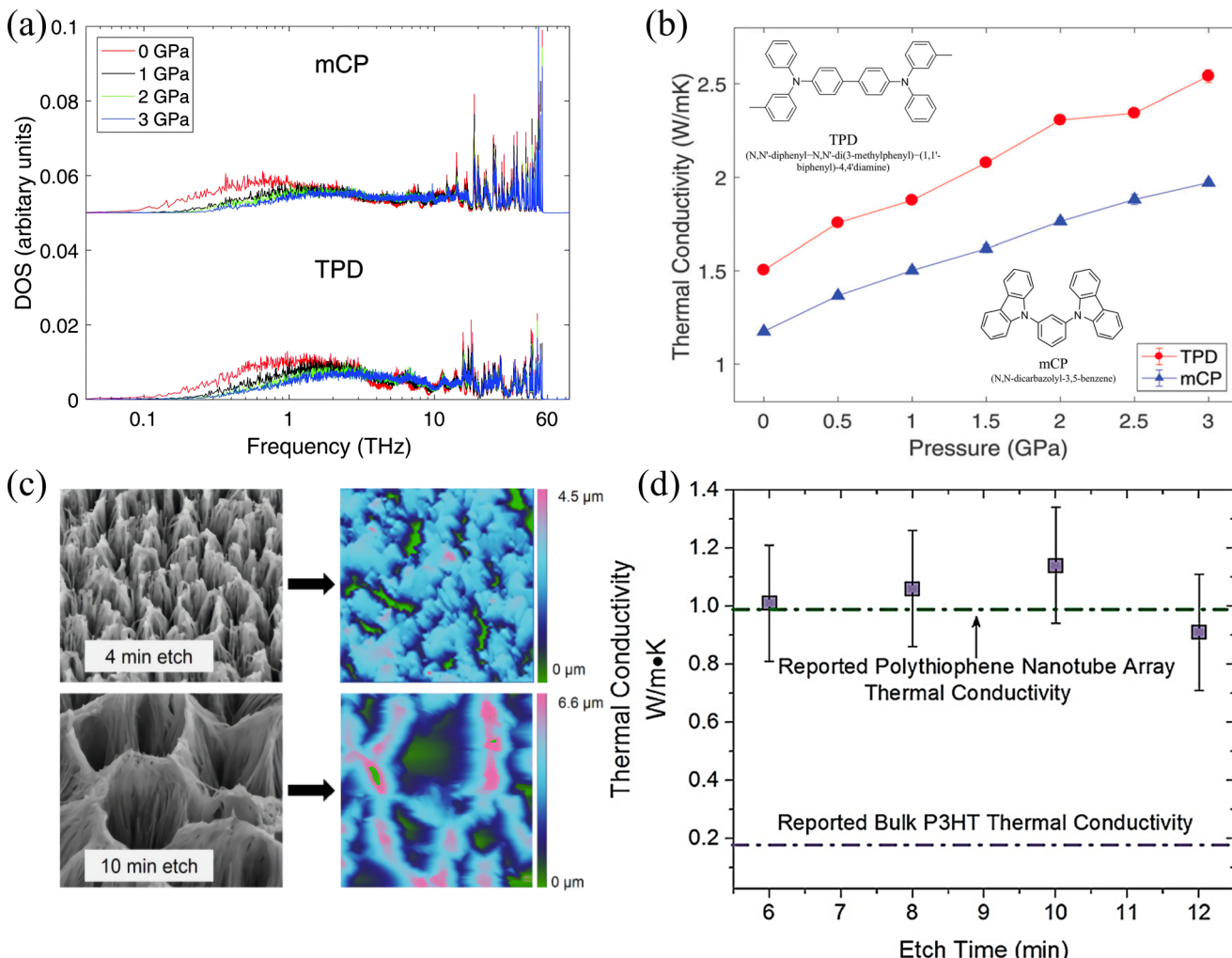


FIG. 6. (a) Vibrational density of states of TPD and mCP at 0, 1, 2, and 3 GPa. (b) Pressure dependent thermal conductivities of TPD and mCP at 300 K.¹⁴⁰ Reproduced with permission from Zhou *et al.*, Phys. Chem. Chem. Phys. **22**, 3058–3065 (2020). Copyright 2020 The PCCP Owner Societies. (c) AFM measurements depicting P3HT nanotube array heights as a function of etch time for an etch time of 4 min and 10 min. (d) Effective thermal conductivity of P3HT [poly(3-hexylthiophene)] nanotube array as a function of etch time.¹⁴³ Reproduced with permission from Smith *et al.*, ACS Nano **9**, 1080–1088 (2015). Copyright 2015 American Chemical Society.

enhancing temperature, and the inelastic phonon scattering may also influence the thermal transport at the interface. Hence, Hopkins and Norris introduced inelastic phonon scattering into the classic DMM and proposed the joint frequency diffuse mismatch model (JFDMM).¹⁵¹ Moreover, to explain the multiple phonons scattering at the interface, an anharmonic inelastic model (AIM) is established by considering the energy and phonon number conservation of all phonon frequencies, of which TBR results are consistent with the experimental results.¹⁵²

However, assumptions of phonon behaviors at the interface in all above theoretical models are simplistic. For the complex interface, such as organic semiconductors and other materials, on account of the vdW interaction at the interface, the inelastic phonon scattering plays an essential role in the interfacial thermal

transport. Moreover, as mentioned above, organic semiconductors have complex morphologies, which tend to form into polycrystal or amorphous structures and introduce some extra phonon scatterings at the interface, such as phonon-defect scattering and phonon-boundary scattering. Thus, it is arduous to accurately predict the TBR between organic semiconductors and other materials by using existing theoretical models. For example, Jin *et al.* experimentally measured the interfacial thermal conductance at the organic semiconductor–metal interface, which proved that predicted values obtained from AMM/DMM were 5–50 times higher than experimental measurement values.¹⁶ Hence, experimental measurement and MD simulation have gradually become important channels to investigate the thermal transport at the interface between organic semiconductors and other materials.

B. Research on organic semiconductor-graphene interface

Graphene, as a representative two-dimensional material, combined with organic semiconductors opens up a new research potential in organic electronics.^{153–158} Therefore, it is crucial to explore the thermal transport mechanism at the organic semiconductor-graphene interface to provide guidance for the thermal management of organic electronic devices.

Previous studies have reported that graphene has extraordinary thermal properties, such as ultrahigh thermal conductivity ($2000\text{--}6000 \text{ W m}^{-1} \text{ K}^{-1}$) and the unique phonon transport behavior, and the underlying physical mechanism has been extensively investigated.¹⁵⁹ The thermal transport of graphene mainly depends on acoustic phonon modes, including the in-plane transverse acoustic (TA) phonon mode, the in-plane longitudinal acoustic (LA) phonon mode, and the out-of-plane acoustic (ZA) phonon mode. The ZA phonon mode plays a dominant role in the thermal transport of graphene, and the contribution to the thermal conductivity can reach $\sim 80\%$.¹⁶⁰ This specific phenomenon can be ascribed to the decoupled phonon modes between ZA and TA/LA.

Phonon is the heat carrier at the organic semiconductor-graphene interface, with a large discrepancy between organic semiconductor and graphene. It can be observed from Fig. 7(a) that phonon DOS of organic semiconductors and graphene are obviously different, leading to diverse phonon vibration properties and the mismatch of phonons, which gives rise to the TBR. In the organic semiconductor-graphene interface, the in-plane and out-of-plane phonons of graphene are coupled owing to the phonon scattering at organic semiconductor atoms, causing thermal resistance in the energy transfer process. Based on the above analysis, the total thermal resistance is composed of the thermal resistance generated by in-plane and out-of-plane coupled phonons of graphene and the thermal resistance generated by out-of-plane phonons of graphene and phonons of organic semiconductors. Wang *et al.* employed the transient heating method in MD simulation to mimic the experimental pump-probe technique to calculate the TBR between graphene and DNTT.¹⁵⁶ In this method, an ultrafast thermal impulse was imposed on graphene as shown in Fig. 7(b), and the thermal energy only could transport from graphene to DNTT during the thermal relaxation process because of the vacuum environment. Thus, the temperature and energy of graphene decreased, the temperature of DNTT increased, and the TBR could be obtained from the energy variation of graphene [Fig. 7(c)]. Calculated results showed that the TBR between graphene and DNTT at 300 K was $5.07 \pm 0.35 \times 10^{-8} \text{ m}^2 \text{ K W}^{-1}$. In general, the thermal conductivity of graphene is a function of phonon MFP, which will elevate with the enhancing system length on account of the increasing long-wavelength (low-frequency) phonons participated in energy transport.^{128,161} However, the previous study has shown that the size effect on the TBR of organic semiconductor-graphene can be neglected, as shown in Fig. 7(d).¹⁵⁶ Although larger graphene size and DNTT thickness can increase the number of low-frequency phonons, the primary energy channel between DNTT and graphene is in the 20–52 THz frequency range [Fig. 7(a)], resulting in the low-frequency phonon with a small contribution, which further causes the size-independent TBR.

Previous works have demonstrated that TBR at the organic semiconductor-graphene interface is sensitive to the temperature and reported a monotonically decreasing relationship between the TBR and the temperature.^{162,163} The increasing temperature will excite more high-frequency phonons, which enlarges phonon transport channels between organic semiconductor and graphene.^{155,156} Moreover, high temperature will shorten the phonon MFP and decompose high-frequency phonons into more low-frequency phonons because of the increasing phonon Umklapp scattering,¹³⁵ which facilitates the phonon coupling of organic semiconductors and graphene. In addition, the vdW interaction at the organic semiconductor-graphene interface has an effect on the interface distance and graphene structure. Larger vdW interaction at the interface will enhance the interfacial thermal transport between organic semiconductor and graphene. Typically, vdW interaction is commonly described by the coupling strength. The study by Ma *et al.* showed that the interfacial thermal conductance between graphene and C_{60} was proportional to the coupling strength, as shown in Fig. 8(a).¹⁵⁷ Furthermore, Wang *et al.* observed a similar variation trend of the TBR between graphene and pentacene with different crystal orientations.¹⁵⁵ On the one hand, the increase of coupling strength directly strengthens the phonon coupling between the organic semiconductor and graphene, which reduces the TBR. On the other hand, the overlapping factor between in-plane and out-of-plane phonons of graphene increases with the enhanced coupling strength [Fig. 8(b)], which enhances in-plane and out-of-plane phonon coupling and contributes to the energy transport of phonons at the interface.

Surface chemical treatment to functionalize graphene will affect the thermal performance of graphene-based organic electronic devices and control the heat transfer capability of different interfaces in the device. Typically, hydrogenation as a surface chemical treatment can change the hybrid type of C atoms from sp^2 hybridization to sp^3 hybridization, which will further impact the phonon transport properties of graphene. Previous studies on thermal properties of DNTT and H-graphene [Fig. 8(c)] reported that as the hydrogen coverage ratio of graphene increases, the TBR first drops sharply and then reaches a constant value and finally increases slightly. At the low-concentration hydrogenation region, introducing the hydrogen atom broadens the phonon DOS of graphene and suppresses the G-band due to the lower mass and higher vibrational frequency of the hydrogen atom, which also promotes the energy conversion between in-plane and out-of-plane phonons of graphene caused by hydrogen atoms as new scattering cores. Furthermore, the interaction between hydrogen atoms on DNTT and graphene can directly improve the interfacial thermal transport. However, at the high-concentration hydrogenation region, a larger high-frequency peak of graphene originating from the hydrogen atom causes the phonon mismatch between DNTT and graphene, which decreases the overlapping of phonon DOS and inhibits the interfacial heat transport. Additionally, structural defects, especially vacancies, are inevitable in fabricating organic semiconductors and graphene, which can impact the thermal transport in them. It has been proved that the TBR at the organic semiconductor-graphene interface is more affected by graphene vacancies. The TBR decreases with the increasing vacancy concentration of graphene [Fig. 8(d)], whereas it is insensitive to the vacancy concentration of

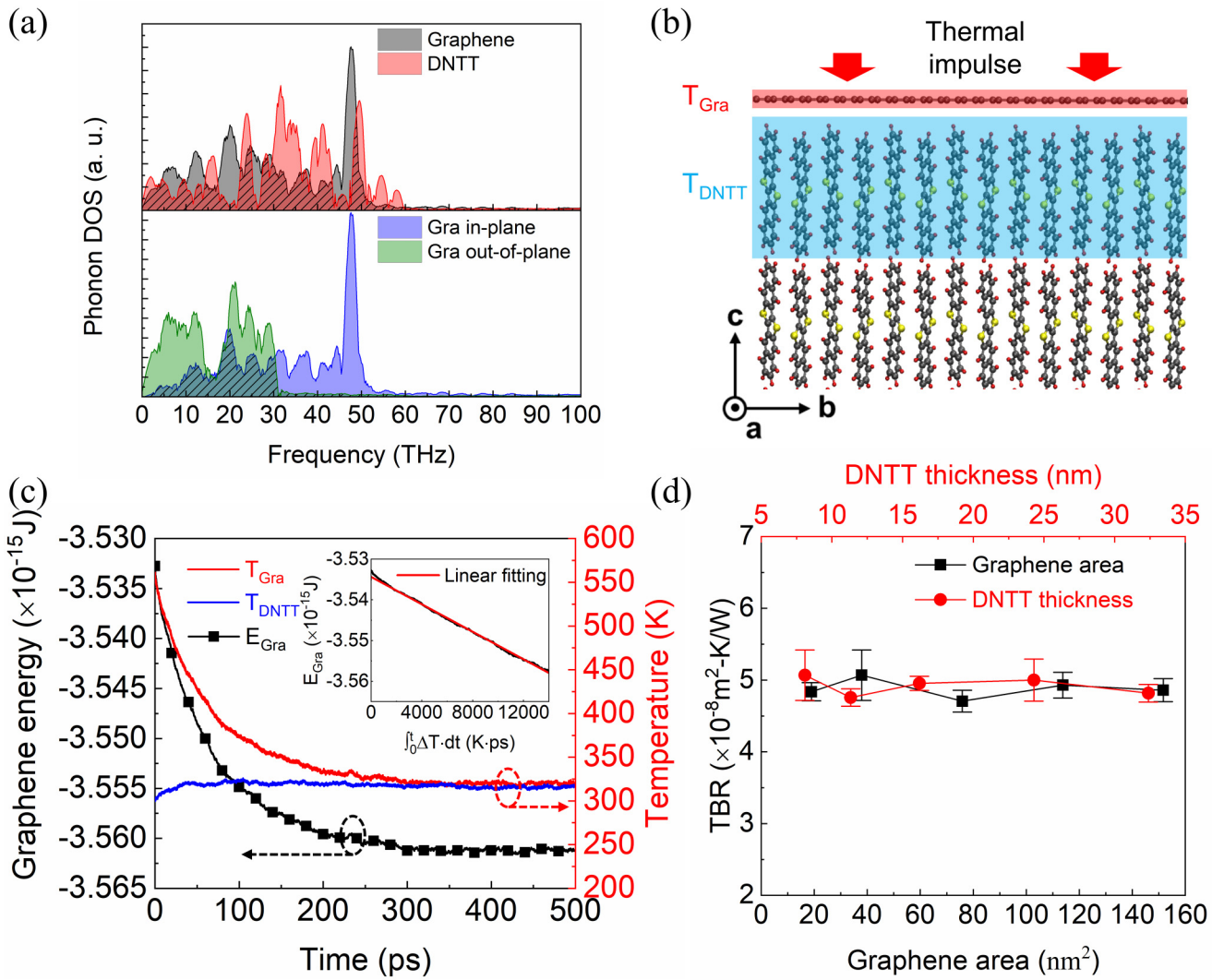


FIG. 7. (a) Phonon DOS of total graphene and DNTT (upper panel), and in-plane and out-of-plane graphene (lower panel). (b) Schematic illustration of the graphene-DNTT heterostructure. (c) Energy evolution of graphene (left y axis) and temperature evolution of graphene and single DNTT layers (right y axis) during the 500 ps relaxation process. (d) TBR variation of graphene and DNTT at different graphene areas and DNTT thicknesses.¹⁵⁶ Reproduced with permission from Wang *et al.*, Phys. Chem. Chem. Phys. **19**, 15933–15941 (2017). Copyright 2017 The PCCP Owner Societies.

organic semiconductors.^{155,156} Vacancies will destroy the perfect sp^2 hybrid lattice structure of graphene and strengthen the extra phonon-vacancy scattering, which lead to the enhanced energy conversion between organic semiconductor and graphene.

C. Research on organic semiconductor-metal interface

In organic electronic devices, metal materials working as electrodes have high thermal conductivity, facilitating the heat transport. However, organic semiconductors acting as active layers usually have low thermal conductivity, easily coming into being the heat accumulation of organic electronic devices. Moreover, organic semiconductors are combined with metals

through vdW interactions and phonons are scattered at the organic semiconductor-metal interface to form a temperature drop, which will impede the heat transport at the organic semiconductor–metal interface. On the one hand, the vdW interaction leads to the lattice vibration mismatch of two materials and strong inelastic phonon scattering. On the other hand, the interfacial energy exchange between the organic semiconductor and the metal electrode largely depends on the interfacial interaction. Therefore, it is of great significance to investigate the heat transport mechanism at the organic semiconductor–metal interface, which is favorable for improving the overall performance of organic electronic devices.

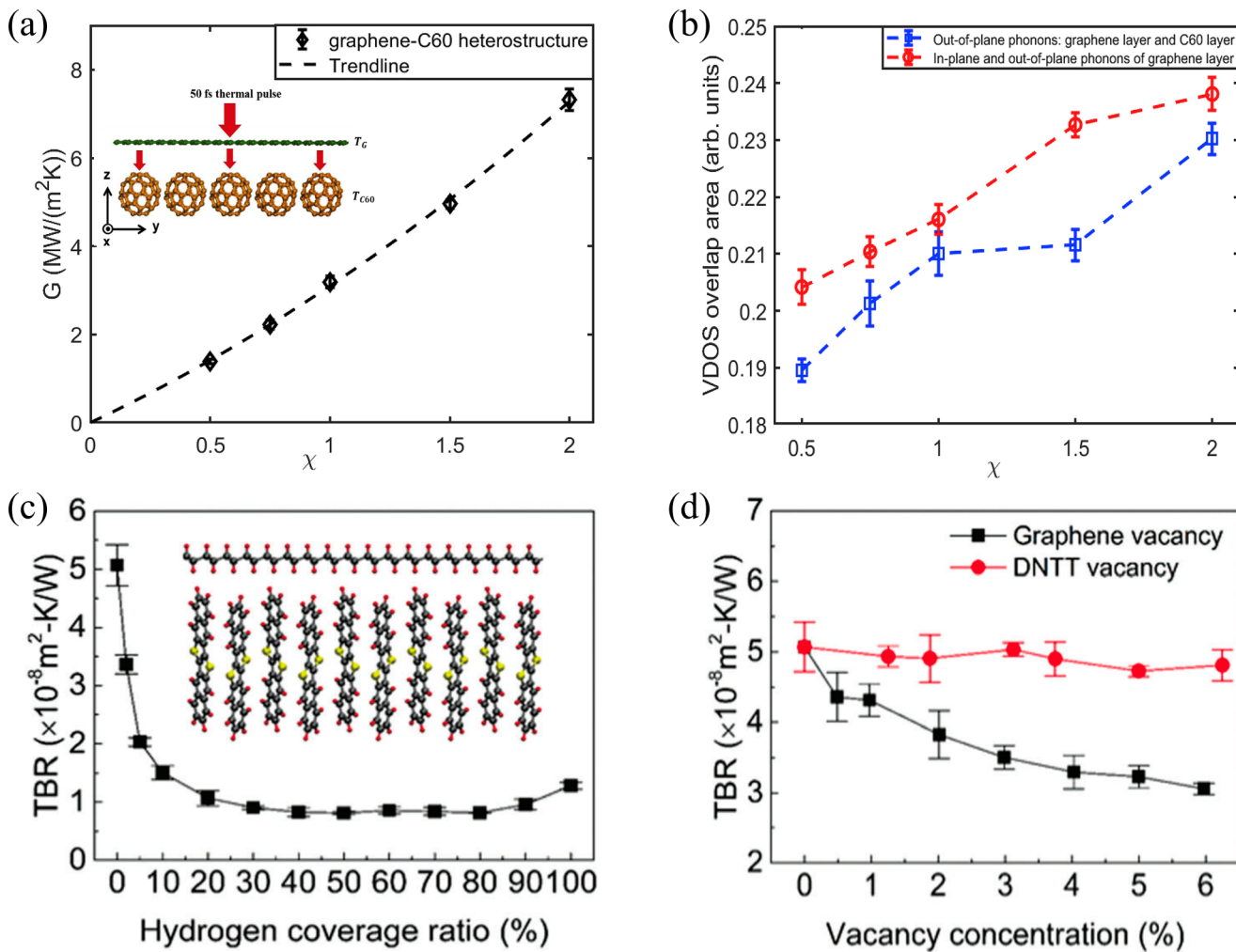


FIG. 8. (a) Interfacial thermal conductance (G) at the graphene–C₆₀ interface as a function of coupling strength (χ) at 300 K. (b) VDOS overlap area of out-of-plane phonons between graphene and C₆₀ as a function of χ at 300 K denoted by blue squares and VDOS overlap area between in-plane and out-of-plane phonons of graphene as a function of χ at 300 K denoted by red circles.¹⁵⁷ Reproduced with permission from Ma *et al.*, Carbon **148**, 196–203 (2019). Copyright 2019 Elsevier. (c) TBR at the DNTT-graphene interface as a function of hydrogen coverage ratio. The inset shows the illustration of the hydrogenated DNTT-graphene heterostructure. (d) TBR at the graphene-DNTT interface as a function of graphene and DNTT vacancy concentrations.¹⁵⁶ Reproduced with permission from Wang *et al.*, Phys. Chem. Chem. Phys. **19**, 15933–15941 (2017). Copyright 2017 The PCCP Owner Societies.

The TBC at the organic semiconductor–metal interface is affected by the discrepancy of phonon behaviors between different materials. The mismatch of phonon DOS between organic semiconductors and metals is much larger than that between organic and organic semiconductors, which leads to the smaller TBC at the semiconductor–metal interface.¹⁶ Jin *et al.* used the 3- ω method to experimentally measure the TBC values between different metals (Ag, Au, Mg, and Al) and organic semiconductor (CuPc) at 300 K and reported that the TBC at CuPc–Al and CuPc–Ag interfaces were 5.0×10^7 and $1.3 \times 10^7 \text{ W m}^{-2} \text{ K}^{-1}$, respectively.^{16,17} Moreover, the TBC between Ag and DNTT interface has been measured by the 3- ω method, which was $8.7 \times 10^6 \text{ W m}^{-2} \text{ K}^{-1}$.⁹⁹ These TBCs at

the organic semiconductor–metal interface are lower than those at organic–organic interfaces (CuPc–C₆₀: $4.5 \times 10^8 \text{ W m}^{-2} \text{ K}^{-1}$,¹⁷ DNTT–DNTT with different crystal orientations: $1.4\text{--}3.1 \times 10^8 \text{ W m}^{-2} \text{ K}^{-1}$).⁶⁴

Organic semiconductors combined with different metals have different interfacial interactions, which possess diverse interfacial heat transport performance. Jin *et al.* indirectly demonstrated the variation of the interfacial interaction strength between CuPc and different metals (Ag, Au, Mg, and Al) using the peel-off experiment, as shown in Fig. 9(a).¹⁶ In this experiment, the CuPc–Ag interface with the highest peel-off degree had the smallest interaction, and the CuPc–Al interface with the lowest peel-off degree had

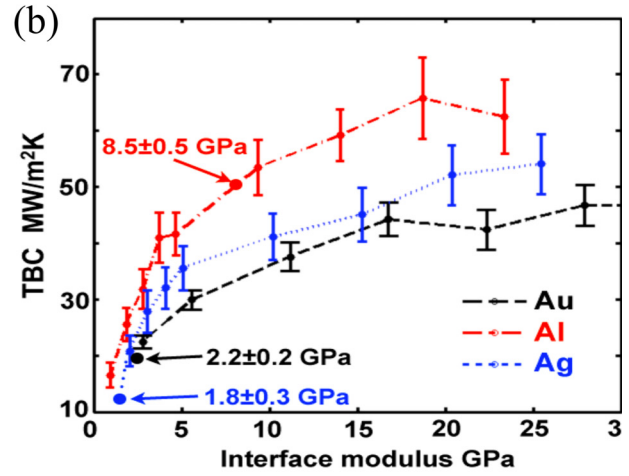
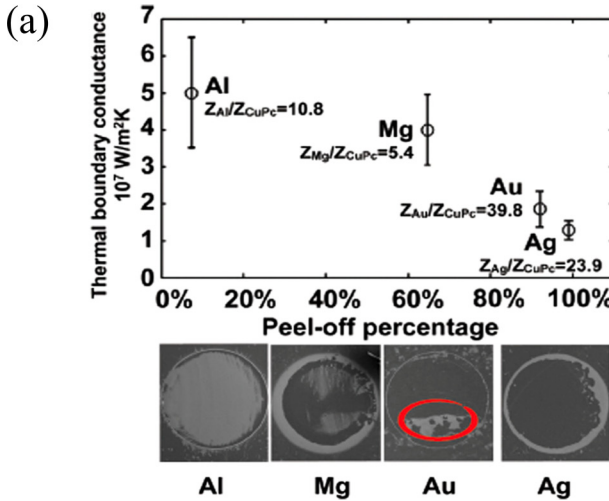


FIG. 9. (a) TBC at CuPc-metal interfaces as a function of peel-off percentage. Peel-off percentage is the ratio of the area of the layered structure that breaks at the CuPc-metal interfaces to the total area covered by metals (upper panel). Scanning electron microscopy (SEM) images of the stacks after peel-off (lower panel). (b) MD calculated TBC at CuPc-Au, CuPc-Al, and CuPc-Ag interfaces as a function of interfacial interaction strength.¹⁶ Reproduced with permission from Jin *et al.*, J. Appl. Phys. **112**, 093503 (2012). Copyright 2012 AIP Publishing LLC.

the largest interaction. After measuring the TBC of different interfaces, they found that the TBC relationship at different interfaces was CuPc-Al > CuPc-Mg > CuPc-Au > CuPc-Ag. This trend is consistent with the relationship of interfacial interactions, which proves that the stronger interfacial interaction leads to the larger TBC. To further verify the effect of the interfacial interaction on TBC, corresponding values at CuPc-Au, CuPc-Al, and CuPc-Ag interfaces with different interactions are studied using MD simulations, which is displayed in Fig. 9(b). The TBC increases with the enhancing interfacial interaction, which is in accord with experimental results.

Moreover, the weak interfacial interaction and the lattice constant mismatch between the organic semiconductor and the metal will affect the growth morphology of the organic semiconductor. Take CuPc-Ag interface as an example [Fig. 10(a)]. For the first layer, organic semiconductor molecules cannot completely cover the metal surface, which is known as the flat molecules, and for the other layers, the molecular arrangement of organic semiconductors exhibits the disordered state.^{164–166} This special growth morphology causes the nonuniform interfacial interaction between organic-metal interfaces, which will affect the thermal transport at the interface.^{164–166} The spatial nonuniformity of organic semiconductor-metal interface is mainly expressed by the following aspects: For organic semiconductor CuPc, the nonuniform interfacial interaction between different atoms of CuPc and Ag can be found in Fig. 10(b) owing to the different effective spring constants. For metal Ag, the nonuniform spatial contact leads to the different interactions at the interface, which affects the phonon DOS of Ag, as shown in Fig. 10(c). Depending on the coverage of organic semiconductors, Ag atoms can be divided into the pack, void, and bulk parts. Unlike the bulk part, the phonon DOS of atoms in pack and void parts are redshifted, and the longitudinal peaks disappear at

5 THz, and specially, the phonon DOS of atoms in the void part shows a more obvious redshift phenomenon because of the non-uniform spatial contact. Thus, the spatial nonuniformity at the organic semiconductor-metal interface has an important effect on the interfacial heat transport. However, theoretical prediction models mentioned in Sec. IV.A neglect this spatial nonuniformity, which cannot be directly used in the calculation of TBC at the organic semiconductor-metal interface. Therefore, based on the existing theoretical model,¹⁶⁷ a model to predict TBC with different spatial nonuniformities has been proposed by correcting the transmission coefficient and considering the effects of diffuse scattering and inelastic scattering, from which TBC results are in good agreement with MD simulation and experimental measurement values.

SAMs are highly ordered molecular assemblies formed by chemisorption and self-organization of long-chain molecules on the surface of specific substrates,¹⁶⁸ which have been widely utilized in surface sensor molecular recognition,^{169,170} interface tension and wettability improvement,¹⁷¹ crystal growth control,¹⁴ and micro/nanoscale surface processing.^{172,173} In addition, researchers also have found that SAMs can improve thermal transport properties of organic semiconductor-metal interfaces. Fan *et al.* adjusted the interfacial thermal transport by adding SAMs with different functional groups between pentacene and Au as shown in Fig. 11(a) and revealed that the ITC at the interface was significantly improved after adding different SAMs.¹⁵ The vibration frequency of Au atoms is mainly distributed in the low-frequency region (<10 THz), while the low-frequency phonon population of pentacene is much less than that of Au, which is depicted in Fig. 11(b). This small phonon overlapping between pentacene and Au is the main reason for the low ITC. Although different SAMs have different functional groups, their vibrational frequencies match better with Au atoms in the low-frequency region than pentacene.

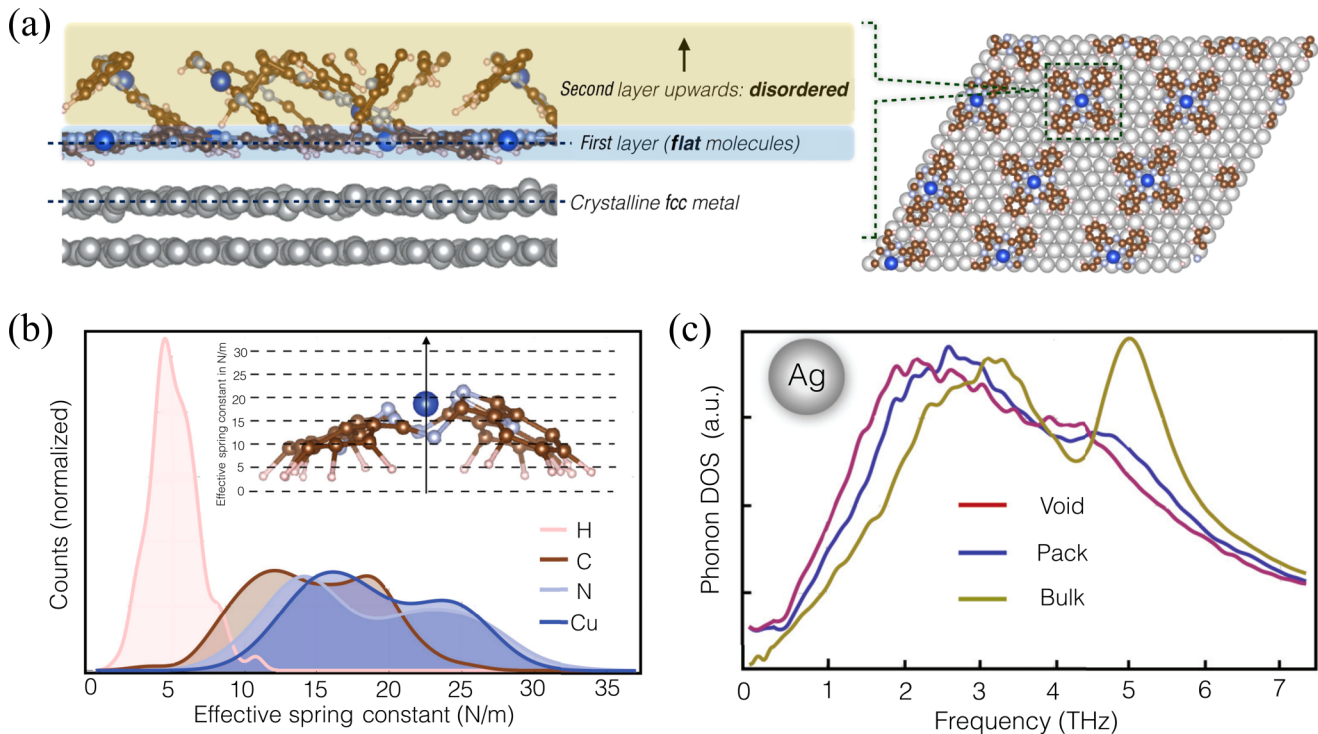


FIG. 10. (a) Side and top views of the CuPc–Ag interface. The metal is in a crystalline state, and CuPc molecules are disordered from the second layer upward, whereas the first-layer molecules lay flat. (b) Effective spring constants of atoms in the first-layer CuPc. (c) Phonon DOS of Ag atoms with different groups. Based on the coverage of organic semiconductors, the metal can be divided into the pack part (covered with CuPc), void part (unconnected with CuPc), and bulk part (Ag atoms far away from the interface).¹⁶⁷ Reproduced with permission from Jin *et al.*, Phys. Rev. B **90**, 054306 (2014). Copyright 2014 American Physical Society.

Furthermore, the overall phonon DOS of SAMs are consistent with pentacene, leading to the SAM molecule playing a role of “phonon bridge” between different materials on both sides of the interface, which broadens the energy transport channel between Au and pentacene. It should be noted that the SAM functional groups with different polarities have different effects on the ITC, and the interface modified by SAM(-COOH) has the highest ITC, which is 11 times larger than the pristine interface. According to previous work,^{174,175} interfacial interaction strength will affect the ITC. It can be seen from the inset of Fig. 11(b) that the SAM(-COOH) modified interface with a stronger polarity corresponds to higher interfacial interaction and adhesion energy, and the SAM(-CH₃) modified interface with weaker polarity has lower interfacial interaction and adhesion energy. This interfacial interaction trend is in accordance with the ITC, which can conclude that different SAM functional groups have different levels of improvement on the ITC, and the stronger polarity of the functional group gives rise to the larger ITC.

D. Research on organic semiconductor-nonmetal interface

Thermal transport at the organic semiconductor–nonmetal interface is mainly divided into the interfacial thermal transport at

the organic–organic semiconductor interface and the organic–inorganic semiconductor interface. For the organic–organic semiconductor interface, the TBR with different crystal orientations and interfacial roughness has been evaluated. On the one hand, the obvious anisotropic thermal conductivity of organic semiconductors results in different TBRs at the organic–organic semiconductor interface with varying crystal orientations. Three representative DNTT–DNTT crystal boundary interfaces, including *a**–*b**; *a**–*c**; and *b**–*c** interfaces, which have the size-independent TBR of 7.00×10^{-9} , 6.15×10^{-9} , and $3.20 \times 10^{-9} \text{ m}^2 \text{ K W}^{-1}$, respectively, and particularly, the *b**–*c** interface shows significantly lower value than other interfaces.⁶⁴ Further investigation has proved that after thermal equilibrium, the molecular structure at the *b**–*c** interface remains stable, while disordered molecular structures at the *a**–*b** and *a**–*c** interfaces are observed. Disordered organic semiconductors cause a strong phonon scattering, which hinders interfacial phonon transport. On the other hand, Xiong *et al.* studied the effect of interfacial roughness on TBR at the CuPc–CuPc interface, in which the TBR at smooth and rough interfaces were 6.5×10^{-9} and $3.85 \times 10^{-7} \text{ m}^2 \text{ K W}^{-1}$, respectively, and subsequently, they calculated the adhesion energy at smooth and rough interfaces by using MD simulation and observed that the adhesion energy at the rough CuPc interface was significantly lower than the smooth interface.¹⁷⁶ The rough surface will cause the increased distance and

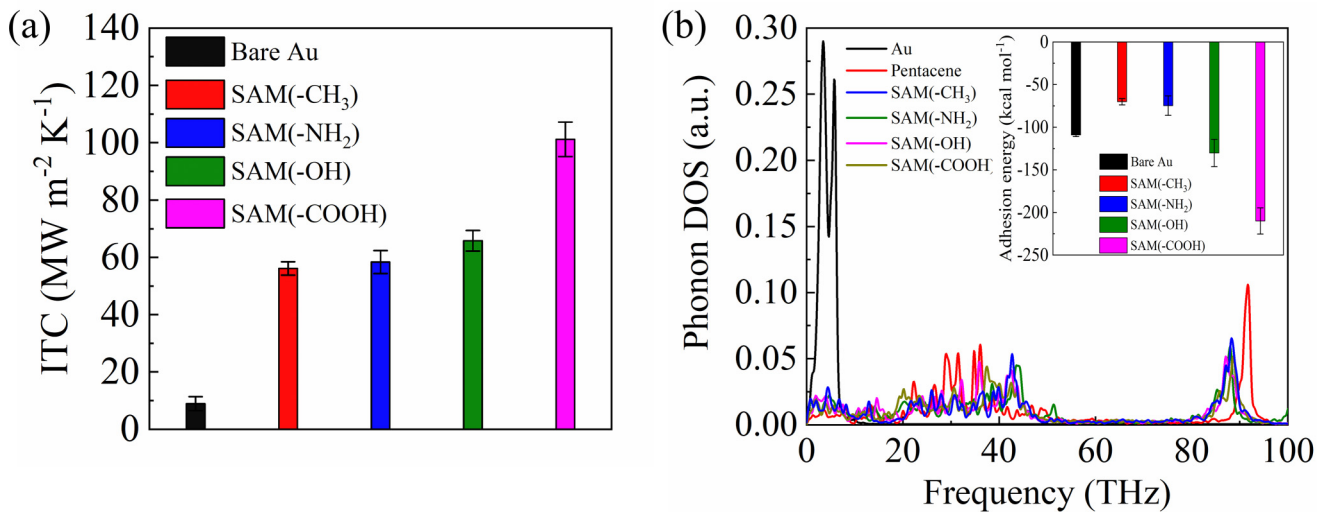


FIG. 11. (a) ITC of the bare Au interface and four SAM-functionalized interfaces. (b) Phonon DOS of Au, different SAMs, and pentacene. The inset represents interfacial adhesion energies of the bare Au interface and four SAM-functionalized interfaces.¹⁵ Reproduced with permission from Fan *et al.*, J. Phys. Chem. C **124**, 16748–16757 (2020). Copyright 2020 American Chemical Society.

decreased effective contact area between interfaces, which reduces the interfacial binding energy and enhanced the TBR. Except for the same organic–organic semiconductors, the TBR at different types of organic–organic semiconductor interfaces has been analyzed. The TBR at the CuPc–C₆₀ interface is $2.2 \times 10^{-9} \text{ m}^2 \text{ K W}^{-1}$, which is in the same order of magnitude as the TBR at the chlorosubphthalocyaninato boron(III) (SubPc)–C₆₀ interface.¹⁶ The better interfacial heat transport at the organic–organic semiconductor interface is the result of higher phonon matching between organic semiconductors. Only a few studies have focused on the interfacial heat transport between organic and inorganic semiconductors. The value of TBR between pentacene and Si measured by Epstein *et al.* was $8.3 \times 10^{-8} \text{ m}^2 \text{ K W}^{-1}$.¹⁴ Moreover, the effects of two types of SAMs with different functional groups [octadecyltrichlorosilane (OTS) and (3-aminopropyl)triethoxysilane (APTES)] on the TBR have been investigated. They found that different SAM substrates led to various roughness on the organic semiconductor surface [Fig. 4(a)]. Although the addition of SAMs impacted the grain size of pentacene crystals grown on Si substrates, SAMs had a slight influence on the TBR of at pentacene–Si interfaces (Si–OTS–pentacene: $8.9 \times 10^{-8} \text{ m}^2 \text{ K W}^{-1}$ and Si–APTES–pentacene: $1.05 \times 10^{-7} \text{ m}^2 \text{ K W}^{-1}$).¹⁴

V. THERMOELECTRIC APPLICATION OF ORGANIC SEMICONDUCTORS

Organic thermoelectric materials as an essential part of organic semiconductors have been used in manufacturing various self-powered devices. Even though great progress for organic thermoelectric materials has been made in recent years, the thermoelectric performance of organic thermoelectric materials needs to be further improved, which can be conducted by modulating the

electrical and thermal properties. In this section, significant achievements on the thermoelectric performance of organic thermoelectric materials are summarized for providing insights into tuning the thermoelectric properties of organic thermoelectric devices.

A. Introduction of thermoelectric application

Thermoelectric materials, which can directly convert the temperature gradient to electric energy, have been regarded as an excellent candidate to solve energy and environmental issues faced by the human society since its significant capability to extract exploitable energy from extensively existed renewable sources of waste heat and solar heat. Moreover, thermoelectric materials can also carry out the reverse conversion from electrics to thermal energy enabled by the Peltier effect, which makes it become a novel refrigeration method without conventional thermodynamic circulation of the working medium. The performance of thermoelectric materials is evaluated by a dimensionless figure of merit, $ZT = S^2 \sigma T / k$, where S is the Seebeck coefficient, σ is the electrical conductivity, T is the absolute temperature, and k is the thermal conductivity. Typical high-performance inorganic thermoelectric materials include Bi₂Te₃, PbTe, SiGe, GeTe, etc., which usually have high electrical conductivity and high Seebeck coefficient. These inorganic materials have been applied in thermoelectric devices with a high figure of merit ($ZT > 2$),¹⁷ and commercial applications are also being continuously promoted. However, many disadvantages of inorganic thermoelectric materials, such as high cost, toxicity, and difficulties in processing, hinder their broad applications.

Contrary to inorganic thermoelectric materials, organic thermoelectric materials can be easily fabricated by solution processing methods in low cost, which makes them more feasible for large-

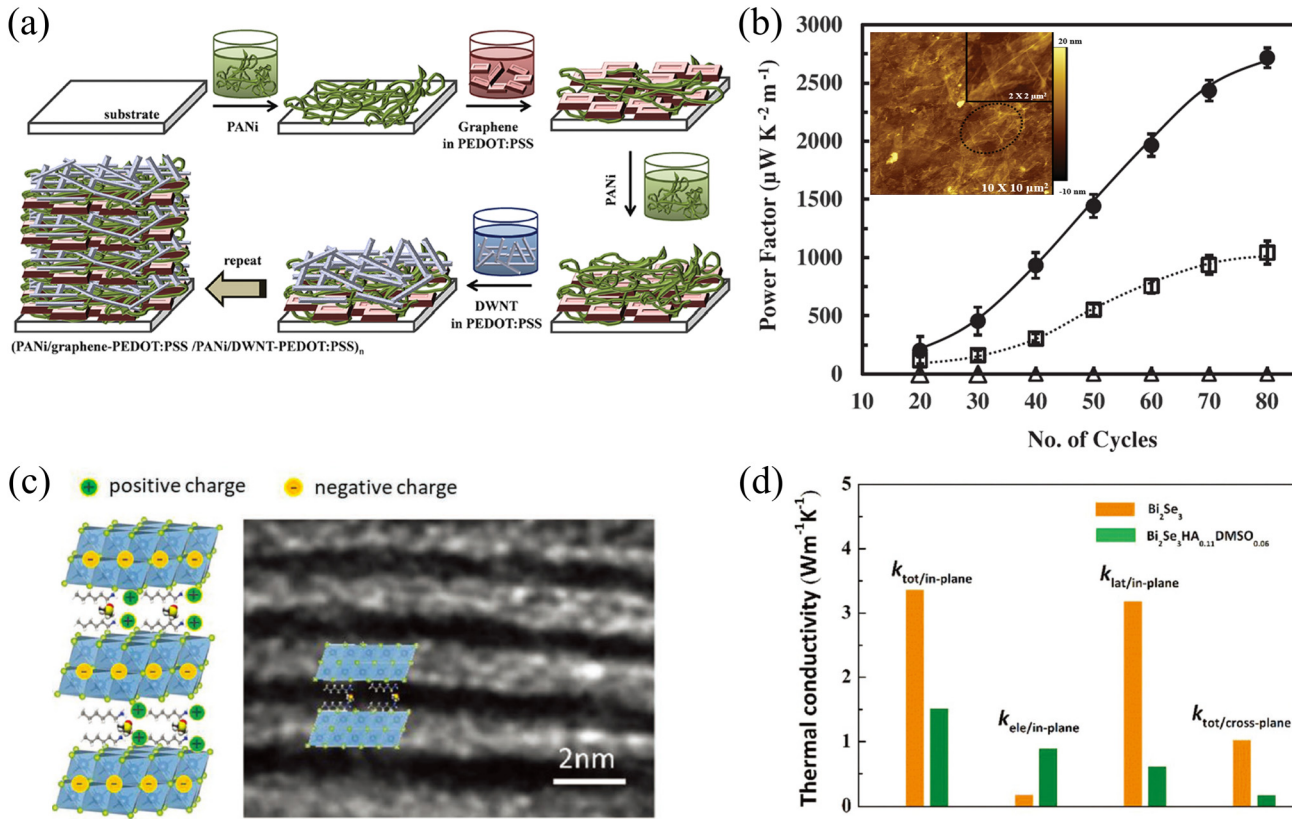


FIG. 12. (a) Schematic illustration of the layer-by-layer deposition process. (b) Electrical conductivity of PANI/DWNT-PEDOT:PSS denoted by open square, and PANI/graphene-PEDOT:PSS/PANI/DWNT-PEDOT:PSS (filled circle) as a function of bilayers or quadlayers (i.e., cycles) deposited on a poly(ethylene terephthalate) substrate.¹⁹⁴ Reproduced with permission from Cho *et al.*, *Adv. Energy Mater.* **6**, 1502168 (2016). Copyright 2016 John Wiley & Sons. (c) Structural representation and TEM image of the cross-sectional $\text{Bi}_2\text{Se}_3\text{HA}_x\text{DMSO}_y$ hybrid. (d) In-plane total thermal conductivity, $k_{\text{tot/in-plane}}$; electrical thermal conductivity, $k_{\text{ele/in-plane}}$; and lattice thermal conductivity, $k_{\text{lat/in-plane}}$, and cross-plane total thermal conductivity $k_{\text{tot/cross-plane}}$ of pristine Bi_2Se_3 and $\text{Bi}_2\text{Se}_3\text{HA}_{0.11}\text{DMSO}_{0.06}$ hybrid.¹⁹⁵ Reproduced with permission from Zong *et al.*, *Adv. Electron. Mater.* **5**, 1800842 (2019). Copyright 2019 John Wiley & Sons.

scale applications. In addition, organic thermoelectric materials can appropriately work in room temperature and low-temperature gradient environments different from the hostile work environment for inorganic thermoelectric materials. The corporation of this feature and advantages of light weight, good flexibility, and biocompatibility make organic thermoelectric materials more applicable to work as the power source of wearable devices and portable devices. Usually, the ZT of organic thermoelectric materials is 2–3 times lower than that of inorganic thermoelectric materials, which is caused by the low electrical conductivity and Seebeck coefficient. However, even though organic thermoelectric materials possess the relatively inferior thermoelectric performance in comparison with their inorganic counterparts, the intrinsically low thermal conductivity of organic thermoelectric materials makes them have huge space for further improvement, particularly, with the intensive attention poured on organic thermoelectric materials, of which performance can be effectively enhanced by various strategies, such as optimizing the organic molecular structure, introducing the

chemical dopant, and designing special microstructure. It is believed that problems faced by organic thermoelectric materials will be solved under the continuous growth of investigation, and organic thermoelectric materials will be exploited in wide applications in the near future.

B. Achievements of organic thermoelectric materials

Since the aforementioned difference of chemical structure between inorganic and organic semiconductor materials, the energy transport in organic thermoelectric materials is more complex than those in inorganic thermoelectric materials, which makes it difficult to model the thermoelectric properties of organic thermoelectric materials.^{178–181} According to the formula of ZT , k is the sum of thermal conductivity contributed by phonons and carriers (electrons or holes), which indicates that evaluation on the thermoelectric performance of organic thermoelectric materials should consider the process of both phonon transport and carrier

transport. With the rapid development of computing power available to researchers and related electronic description theories, researchers can calculate different parameters through various calculation methods based on different physical frameworks to evaluate the thermoelectric performance of organic thermoelectric materials. Up to now, the thermoelectric performance of many thermoelectric materials, including organic molecular crystals, crystalline conjugated polymers,¹⁸² transition metal coordination polymers,^{183,184} and organic-inorganic hybrid perovskites,¹⁸⁵ has been investigated theoretically. For instance, in the beginning, Wang *et al.* used the constant relaxation time approximation to estimate the scattering process of electrons by the phonons, impurities, or other defects,¹⁸⁶ but later, they first used the deformation potential theory to obtain the electron relaxation time in phthalocyanine and metal phthalocyanines by calculating the electron-phonon scattering.¹⁸⁷ After that, they used this scheme to explore the thermoelectric performance of a series of organic semiconductors, including the P3HT, PEDOT, and C_n-BTBTs.^{61,188}

In the past few decades, many outstanding experimental breakthroughs in the thermoelectric performance of organic thermoelectric materials have attracted extensive attention.^{75,83} At present, PEDOT-based organic systems are the most extensively and systematically studied organic thermoelectric materials, which are also the most high-performance organic thermoelectric materials. PEDOT can be fabricated by many methods, including *in situ* chemical polymerization, vapor phase chemical polymerization, chemical vapor deposition, electropolymerization, and dispersion polymerization, which makes various methods to modulate thermoelectric properties of PEDOT-based organic systems. In 2011, Bubnova *et al.* used iron(III) tris-p-toluenesulphonate to oxidize the 3,4-ethylenedioxythiophene (EDOT) monomers and directly polymerized the PEDOT:Tos. The measured electrical conductivity, Seebeck coefficient, and power factor of PEDOT:Tos at room temperature were 300 S cm⁻¹, 40 μ V K⁻¹, and 38 μ W m⁻¹ K⁻², respectively.⁸³ Afterward, they exposed the PEDOT:Tos in tetrakis (dimethylamino)ethylene (TDAE) vapor to reduce it, and the oxidation level of PEDOT:Tos was regulated. Thermoelectric properties varied with the oxidation level, and the thermal conductivity of PEDOT:Tos film was measured to be 0.37 ± 0.07 W m⁻¹ K⁻¹ by the 3- ω method. Consequently, the maximum value of *ZT* was obtained to be 0.25. The PEDOT:PSS system is another important part of PEDOT-based materials. In the PEDOT:PSS system, PSS plays the role of a dopant and acts as a stabilizer. The repulsive interaction caused by the extra negative charge of PSS enables PEDOT:PSS to steadily suspend in an aqueous solution.¹⁸⁹ Mengistie *et al.* used formic acid as a secondary dopant to optimize the PEDOT:PSS, and the electrical conductivity and the power factor were enhanced to 1900 S cm⁻¹ and 80.6 μ W m⁻¹ K⁻².¹⁹⁰

Apart from the PEDOT, some other organic thermoelectric materials such as polythiophene, polyaniline, polypyrrole, metalorganic coordination polymers, and small molecules, are also be investigated to tap their potential for thermoelectric application. Yuan *et al.* investigated the effect of the side alkyl group in PTbT-Tos, and they found that polymers with a short alkyl group had higher electrical conductivity and power factor.¹⁹¹ Qu *et al.* fabricated P3HT films with highly oriented morphology based on the organic small molecule epitaxy of 1,3,5-trichlorobenzene

(TCB),¹³⁷ and the obtained high power factor, low thermal conductivity, and figure of merit were 62.4μ W m⁻¹ K⁻², 0.23 W m⁻¹ K⁻¹, and 0.1 at 365 K, respectively. Metalorganic coordination polymers represent the highest level of n-type organic thermoelectric materials. The coordination polymer formed by ethylenetetrathiolate and nickel is the first high-performance n-type organic thermoelectric material because of the thermal conductivity of 0.4–0.5 W m⁻¹ K⁻¹ and high value of *ZT* ≈ 0.3,¹⁹² which makes n-type organic thermoelectric materials have comparable performance with p-type organic thermoelectric materials. On the other hand, small molecule thermoelectric materials, such as polydopamine, DNTT, C8BTBT, and C₆₀, possess the Seebeck coefficient ranging from 1 to 100 mV K⁻¹,¹⁹³ showing the great potential of these molecules to thermoelectric applications as well.

Except for material systems completely composed of organics, hybrid organic-inorganic thermoelectric materials also have achieved remarkable thermoelectric performance. Popular inorganic materials involved in hybrid systems include graphene, carbon nanotubes, typical inorganic thermoelectric materials, and metals. Cho *et al.* fabricated the hybrid organic-inorganic film comprised of PANI, graphene, PEDOT:PSS, and double-walled carbon nanotube using the layer-by-layer assembly technique [Fig. 12(a)].¹⁹⁴ They investigated the effect of deposition repeating cycles on thermoelectric properties. The electric conductivity and Seebeck coefficient continuously increased with the augmentation of deposition repeating cycles, and finally, the power factor reached an extremely high value of 2710 μ W m⁻¹ K⁻² [Fig. 12(b)]. On the contrary, reducing the thermal conductivity is another pathway to enhance thermoelectric performance, whereas the intrinsically low thermal conductivity of organic materials leaves limited space to reduce their thermal conductivity further. Some studies constructed specific microstructures in hybrid organic-inorganic materials to enhance the phonon scattering process, which ulteriorly reduces thermal conductivity. For example, superlattices composed of the alternate assembly of organic and inorganic materials, where the inorganics is Bi₂Se₃ and the organic layers are comprised of a random mixture of HA and DMSO [Fig. 12(c)], can significantly reduce thermal conductivity of hybrid organic-inorganic materials. In comparison with Bi₂Se₃, the in-plane and cross-plane thermal conductivities of obtained Bi₂Se₃HA_{0.11}DMSO_{0.06} are remarkably decreased from 3.37 to 1.52 W m⁻¹ K⁻¹ and from 1.03 to 0.17 W m⁻¹ K⁻¹ [Fig. 12(d)], respectively, which demonstrate that the superlattice structure can effectively impede the thermal transport and contribute to the large improvement of the *ZT* value. The synthesized hybrid organic-inorganic material of Bi₂Se₃HA_{0.11}DMSO_{0.06} possesses the *ZT* value of 0.187, which is elevated by about 78% compared with Bi₂Se₃.¹⁹⁵

VI. SUMMARY AND OUTLOOK

In conclusion, understanding thermal transport in organic semiconductors is vital to improve the thermal management in high-performance organic electronics and boost the thermoelectric performance of organic thermoelectric materials. In this Perspective, based on a comprehensive summary of the research on thermal transport of organic semiconductors, we have reached the following conclusions:

- (1) Thermal conductivities of organic semiconductors are generally below $1 \text{ W m}^{-1} \text{ K}^{-1}$ and much lower than that of inorganic counterparts. The weak strength of the intermolecular interaction in organic semiconductors makes their thermal properties be influenced by many factors including internal and external factors. Internal factors, such as molecular chemical structure, molecular packing, defects, and film morphology, closely related to intrinsic features of organic semiconductors, create impacts on the degree of order, phonon transport channel, and phonon scattering intensity. External influencing factors, including the temperature and the pressure relating to the environment or human controlled factor, affect the phonon Umklapp scattering and the intermolecular equilibrium space to exert diverse influences on thermal conductivity of organic semiconductors. Moreover, the preparation method can bring about impacts on the molecular packing, defects, and film morphology and subsequently tune the thermal conductivity.
- (2) Interfacial thermal transport is crucial to the overall heat dissipation capability of organic electronics. The mismatch of lattice vibration between materials at two sides of interface, interfacial interaction strength, and microscopic structures at the interface mainly affect the interfacial thermal transport of organic semiconductor-based interfaces. A large mismatch of lattice vibration between organic semiconductors and other inorganic materials leads to inferior interfacial thermal transport, while the well vibrational matched organic–organic semiconductors interfaces have relatively good interfacial thermal transport. Increasing the interfacial interaction strength can directly enhance interfacial heat exchange. Microscopic structures, such as surface roughness, nonuniformity of contacting, and disordered structure near the interface, substantially affect the mismatch of lattice vibration and interfacial bonding strength, which then regulate the interfacial thermal transport.
- (3) In contrast to the heat transfer enhancement, investigations on organic thermoelectric materials aim at reducing thermal conductivity as much as possible. At present, PEDOT is the most successful organic thermoelectric material because of the high performance and good processability for the solution processing method. Through modulating the molecular configuration and constructing specific phonon transport impeding structures, the desired thermoelectric performance has been achieved in many organic material systems.

Compared to the wealth of research on inorganic counterparts, studies related to thermal transport in organic semiconductors are inadequate, leaving many unilluminated corners to be explored. The inadequate and incomplete understanding of thermal transport in organic semiconductor-based material systems may hinder in-depth applications in the future. Several important points and research areas that deserve further exploration are summarized as follows:

- (1) As aforementioned, organic semiconductors can be in monocrystal, polycrystalline, or amorphous structures. The thermal conductivity of single crystal provides a baseline on determining the thermal conductivity of organic semiconductors with other structures. However, there is currently no precise model

to establish a relationship on thermal conductivities among different organic semiconductor structures and quantitatively describe the effect of crystallinity on thermal conductivity. Moreover, the scattering between charge carrier and phonon plays an important role in evaluating the thermal conductivity of heavily doped organic semiconductors. Although the electron–phonon scattering in inorganic semiconductors has been concerned, investigations on the coupling mechanism between charge transport and phonon transport in heavily doped organic semiconductors are still scarce, which is in urgent need of research. Meanwhile, the current research mainly focuses on organic semiconductor thin films, and there are a few studies on the intramolecular thermal transport in a single organic semiconductor molecule. Particularly for polymer organic semiconductors, the effects of molecular folding and twisting on the intramolecular thermal transport are also necessary to be exploited.

- (2) The interfacial thermal transport at organic semiconductor-based interfaces can be influenced by many factors, including mismatch of lattice vibration, interfacial interaction strength, and microscopic structures. Moreover, existing theoretical models for describing interfacial thermal transport fail to accurately evaluate the thermal transport at organic semiconductor-based interfaces. Effects from various influencing factors on the interfacial thermal transport should be systematically considered for the establishment of a new and applicable interfacial thermal transport model. In addition, the weak interfacial vdW interaction between organic semiconductors and other materials easily gives rise to disordered structures at the interface, which inevitably leads to intense phonon scattering at the interface. More importantly, poor match of phonon properties exists between the organic semiconductors and other materials at the interface. Therefore, it is necessary to seek for how to adjust the arrangement of organic semiconductors at the interface to improve the interfacial phonon transmission capability, thereby reducing the interfacial thermal resistance.
- (3) For organic thermoelectric materials, discovering novel organic thermoelectric materials with high intrinsic ZT values is the most significant progress. Currently, existing studies on thermoelectric properties mainly focus on electrical conductivity and Seebeck coefficient, but the influence of various factors on thermal conductivity has not been studied effectively. Furthermore, inorganic conductive materials in hybrid organic–inorganic systems promote the electric transport process increasing the electric conductivity but also result in the enhancement of thermal conductivity. More investigations into the energy transport mechanism between organic and inorganic components are needed to modulate electrical and thermal properties separately.

We anticipate that this Perspective will not only provide fundamental insight into the thermal transport of organic semiconductors but also enlighten the development of new organic semiconductors for applications, which may require collaboration between researchers from different fields using their expertise.

ACKNOWLEDGMENTS

X.W. gratefully acknowledges financial support from the National Natural Science Foundation of China (No. 51806123), the Guangdong Basic and Applied Basic Research Foundation (No. 2020A1515010686), the Shenzhen Science and Technology Program (No. RCBS20200714114817106), the Shandong Provincial Postdoctoral Innovation Program (No. 201902001), and the Young Scholars Program of Shandong University. J.Z. gratefully acknowledges support from the NVIDIA AI Technology Center.

DATA AVAILABILITY

Data sharing is not applicable to this article as no new data were created or analyzed in this study.

AUTHOR DECLARATIONS

Conflict of Interest

There are no conflicts of interest to declare.

REFERENCES

- ¹H. Ling, S. Liu, Z. Zheng, and F. Yan, "Organic flexible electronics," *Small Methods* **2**, 1800070 (2018).
- ²Y. Wang, L. Sun, C. Wang, F. Yang, X. Ren, X. Zhang, H. Dong, and W. Hu, "Organic crystalline materials in flexible electronics," *Chem. Soc. Rev.* **48**, 1492–1530 (2019).
- ³P. C. Y. Chow and T. Someya, "Organic photodetectors for next-generation wearable electronics," *Adv. Mater.* **32**, 1902045 (2020).
- ⁴J.-H. Bahk, H. Fang, K. Yazawa, and A. Shakouri, "Flexible thermoelectric materials and device optimization for wearable energy harvesting," *J. Mater. Chem. C* **3**, 10362–10374 (2015).
- ⁵H. Klauk, U. Zschieschang, J. Pflaum, and M. Halik, "Ultralow-power organic complementary circuits," *Nature* **445**, 745–748 (2007).
- ⁶J. Borges-González, C. J. Koushoeff, and C. B. Nielsen, "Organic semiconductors for biological sensing," *J. Mater. Chem. C* **7**, 1111–1130 (2019).
- ⁷G. Lanzani, "Organic electronics meets biology," *Nat. Mater.* **13**, 775–776 (2014).
- ⁸C. Wang, H. Dong, L. Jiang, and W. Hu, "Organic semiconductor crystals," *Chem. Soc. Rev.* **47**, 422–500 (2018).
- ⁹J. Mei, Y. Diao, A. L. Appleton, L. Fang, and Z. Bao, "Integrated materials design of organic semiconductors for field-effect transistors," *J. Am. Chem. Soc.* **135**, 6724–6746 (2013).
- ¹⁰G. Schweicher, Y. Olivier, V. Lemaur, and Y. H. Geerts, "What currently limits charge carrier mobility in crystals of molecular semiconductors?," *Isr. J. Chem.* **54**, 595–620 (2014).
- ¹¹P. G. Le Comber and W. E. Spear, "Electronic transport in amorphous silicon films," *Phys. Rev. Lett.* **25**, 509–511 (1970).
- ¹²Z.-P. Fan, X.-Y. Li, G. E. Purdum, C.-X. Hu, X. Fei, Z.-F. Shi, C.-L. Sun, X. Shao, Y.-L. Loo, and H.-L. Zhang, "Enhancing the thermal stability of organic field-effect transistors by electrostatically interlocked 2D molecular packing," *Chem. Mater.* **30**, 3638–3642 (2018).
- ¹³A. Nigam, D. Kabra, T. Garg, M. Premaratne, and V. R. Rao, "Insight into the charge transport and degradation mechanisms in organic transistors operating at elevated temperatures in air," *Org. Electron.* **22**, 202–209 (2015).
- ¹⁴J. Epstein, W.-L. Ong, C. J. Bettinger, and J. A. Malen, "Temperature dependent thermal conductivity and thermal interface resistance of pentacene thin films with varying morphology," *ACS Appl. Mater. Interfaces* **8**, 19168–19174 (2016).
- ¹⁵H. Fan, M. Wang, D. Han, J. Zhang, J. Zhang, and X. Wang, "Enhancement of interfacial thermal transport between metal and organic semiconductor using self-assembled monolayers with different terminal groups," *J. Phys. Chem. C* **124**, 16748–16757 (2020).
- ¹⁶Y. Jin, C. Shao, J. Kieffer, K. P. Pipe, and M. Shtein, "Origins of thermal boundary conductance of interfaces involving organic semiconductors," *J. Appl. Phys.* **112**, 093503 (2012).
- ¹⁷Y. Jin, A. Yadav, K. Sun, H. Sun, K. P. Pipe, and M. Shtein, "Thermal boundary resistance of copper phthalocyanine-metal interface," *Appl. Phys. Lett.* **98**, 093305 (2011).
- ¹⁸R. J. Stevens, A. N. Smith, and P. M. Norris, "Measurement of thermal boundary conductance of a series of metal-dielectric interfaces by the transient thermoreflectance technique," *J. Heat. Transfer* **127**, 315–322 (2005).
- ¹⁹H. Sun, Y. Gui, H. Wei, Y. Long, Q. Wang, and C. Tang, "DFT study of SF₆ decomposed products on Pd-TiO₂: Gas sensing mechanism study," *Adsorption* **25**, 1643–1653 (2019).
- ²⁰H. Derouiche and V. Djara, "Impact of the energy difference in LUMO and HOMO of the bulk heterojunctions components on the efficiency of organic solar cells," *Sol. Energy Mater. Sol. Cells* **91**, 1163–1167 (2007).
- ²¹B.-G. Kim, X. Ma, C. Chen, Y. Ie, E. W. Coir, H. Hashemi, Y. Aso, P. F. Green, J. Kieffer, and J. Kim, "Energy level modulation of HOMO, LUMO, and bandgap in conjugated polymers for organic photovoltaic applications," *Adv. Funct. Mater.* **23**, 439–445 (2013).
- ²²F. Rissner, G. M. Rangger, O. T. Hofmann, A. M. Track, G. Heimel, and E. Zojer, "Understanding the electronic structure of metal/SAM/organic-semiconductor heterojunctions," *ACS Nano* **3**, 3513–3520 (2009).
- ²³Y. Yuan, G. Giri, A. L. Ayzner, A. P. Zombeck, S. C. B. Mannsfeld, J. Chen, D. Nordlund, M. F. Toney, J. Huang, and Z. Bao, "Ultra-high mobility transparent organic thin film transistors grown by an off-centre spin-coating method," *Nat. Commun.* **5**, 3005 (2014).
- ²⁴H. Minemawari, T. Yamada, H. Matsui, J. Tsutsumi, S. Haas, R. Chiba, R. Kumai, and T. Hasegawa, "Inkjet printing of single-crystal films," *Nature* **475**, 364–367 (2011).
- ²⁵G. Giri, E. Verploegen, S. C. B. Mannsfeld, S. Atahan-Evrenk, D. H. Kim, S. Y. Lee, H. A. Becerril, A. Aspuru-Guzik, M. F. Toney, and Z. Bao, "Tuning charge transport in solution-sheared organic semiconductors using lattice strain," *Nature* **480**, 504–508 (2011).
- ²⁶J. Liu, H. Zhang, H. Dong, L. Meng, L. Jiang, L. Jiang, Y. Wang, J. Yu, Y. Sun, W. Hu, and A. J. Heeger, "High mobility emissive organic semiconductor," *Nat. Commun.* **6**, 10032 (2015).
- ²⁷O. D. Jurchescu, M. Popinciuc, B. J. Van Wees, and T. T. Palstra, "Interface-controlled, high-mobility organic transistors," *Adv. Mater.* **19**, 688–692 (2007).
- ²⁸T. Okamoto, S. Kumagai, E. Fukuzaki, H. Ishii, G. Watanabe, N. Niitsu, T. Annaka, M. Yamagishi, Y. Tani, H. Sugiura, T. Watanabe, S. Watanabe, and J. Takeya, "Robust, high-performance n-type organic semiconductors," *Sci. Adv.* **6**, eaaz0632 (2020).
- ²⁹X. Gao and Y. Hu, "Development of n-type organic semiconductors for thin film transistors: A viewpoint of molecular design," *J. Mater. Chem. C* **2**, 3099–3117 (2014).
- ³⁰J. T. E. Quinn, J. Zhu, X. Li, J. Wang, and Y. Li, "Recent progress in the development of n-type organic semiconductors for organic field effect transistors," *J. Mater. Chem. C* **5**, 8654–8681 (2017).
- ³¹C. Zhang, Y. Zang, F. Zhang, Y. Diao, C. R. McNeill, C.-a. Di, X. Zhu, and D. Zhu, "Pursuing high-mobility n-type organic semiconductors by combination of "molecule-framework" and "side-chain" engineering," *Adv. Mater.* **28**, 8456–8462 (2016).
- ³²J. Veres, S. Ogier, G. Lloyd, and D. de Leeuw, "Gate insulators in organic field-effect transistors," *Chem. Mater.* **16**, 4543–4555 (2004).
- ³³S. Verlaak, S. Steudel, P. Heremans, D. Janssen, and M. S. Deleuze, "Nucleation of organic semiconductors on inert substrates," *Phys. Rev. B* **68**, 195409 (2003).
- ³⁴A. Virkar, S. Mannsfeld, J. H. Oh, M. F. Toney, Y. H. Tan, G.-y. Liu, J. C. Scott, R. Miller, and Z. Bao, "The role of OTS density on pentacene and C₆₀ nucleation, thin film growth, and transistor performance," *Adv. Funct. Mater.* **19**, 1962–1970 (2009).

- ³⁵S. Steudel, D. Janssen, S. Verlaak, J. Genoe, and P. Heremans, "Patterned growth of pentacene," *Appl. Phys. Lett.* **85**, 5550–5552 (2004).
- ³⁶Y. Fan, J. Liu, W. Hu, Y. Liu, and L. Jiang, "The effect of thickness on the optoelectronic properties of organic field-effect transistors: Towards molecular crystals at monolayer limit," *J. Mater. Chem. C* **8**, 13154–13168 (2020).
- ³⁷J. H. Van Der Merwe, "Theoretical considerations in growing uniform epilayers," *Interface Sci.* **1**, 77–86 (1993).
- ³⁸S.-Y. Kwak, C. G. Choi, and B.-S. Bae, "Effect of surface energy on pentacene growth and characteristics of organic thin-film transistors," *Electrochim. Solid State* **12**, G37–G39 (2009).
- ³⁹Z. Wang, X. Ren, C. Fan, Y. H. Chang, H. Li, H. Chen, S. P. Feng, S. Shi, and P. K. L. Chan, "Low cost universal high-k dielectric for solution processing and thermal evaporation organic transistors," *Adv. Mater. Interfaces* **1**, 1300119 (2014).
- ⁴⁰S. Steudel, S. De Vusser, S. De Jonge, D. Janssen, S. Verlaak, J. Genoe, and P. Heremans, "Influence of the dielectric roughness on the performance of pentacene transistors," *Appl. Phys. Lett.* **85**, 4400–4402 (2004).
- ⁴¹C. D. Dimitrakopoulos and D. J. Mascaro, "Organic thin-film transistors: A review of recent advances," *IBM J. Res. Dev.* **45**, 11–27 (2001).
- ⁴²P. C. Chang, S. E. Molesa, A. R. Murphy, J. M. J. Fréchet, and V. Subramanian, "Inkjetted crystalline single monolayer oligothiophene OTFTs," *IEEE Trans. Electron Dev.* **53**, 594–600 (2006).
- ⁴³C. D. Dimitrakopoulos and P. R. L. Malenfant, "Organic thin film transistors for large area electronics," *Adv. Mater.* **14**, 99–117 (2002).
- ⁴⁴J. Mei, D. H. Kim, A. L. Ayzner, M. F. Toney, and Z. Bao, "Siloxane-terminated solubilizing side chains: Bringing conjugated polymer backbones closer and boosting hole mobilities in thin-film transistors," *J. Am. Chem. Soc.* **133**, 20130–20133 (2011).
- ⁴⁵B. Peng, S. Huang, Z. Zhou, and P. K. L. Chan, "Solution-processed monolayer organic crystals for high-performance field-effect transistors and ultrasensitive gas sensors," *Adv. Funct. Mater.* **27**, 1700999 (2017).
- ⁴⁶W. Ou-Yang, T. Uemura, K. Miyake, S. Onishi, T. Kato, M. Katayama, M. Kang, K. Takimiya, M. Ikeda, H. Kuwabara, M. Hamada, and J. Takeya, "High-performance organic transistors with high-k dielectrics: A comparative study on solution-processed single crystals and vacuum-deposited polycrystalline films of 2,9-didecyl-dinaphtho[2,3-b;2',3'-f]thieno[3,2-b]thiophene," *Appl. Phys. Lett.* **101**, 223304 (2012).
- ⁴⁷K. Nakayama, Y. Hirose, J. Soeda, M. Yoshizumi, T. Uemura, M. Uno, W. Li, M. J. Kang, M. Yamagishi, Y. Okada, E. Miyazaki, Y. Nakazawa, A. Nakao, K. Takimiya, and J. Takeya, "Patternable solution-crystallized organic transistors with high charge carrier mobility," *Adv. Mater.* **23**, 1626–1629 (2011).
- ⁴⁸J. S. Kim, B. J. Kim, Y. J. Choi, M. H. Lee, M. S. Kang, and J. H. Cho, "An organic vertical field-effect transistor with underside-doped graphene electrodes," *Adv. Mater.* **28**, 4803–4810 (2016).
- ⁴⁹M. Muccini, "A bright future for organic field-effect transistors," *Nat. Mater.* **5**, 605–613 (2006).
- ⁵⁰S. Yuvaraja, A. Nawaz, Q. Liu, D. Dubal, S. G. Surya, K. N. Salama, and P. Sonar, "Organic field-effect transistor-based flexible sensors," *Chem. Soc. Rev.* **49**, 3423–3460 (2020).
- ⁵¹B. Geffroy, P. le Roy, and C. Prat, "Organic light-emitting diode (OLED) technology: Materials, devices and display technologies," *Polym. Int.* **55**, 572–582 (2006).
- ⁵²F. Guo, A. Karl, Q.-F. Xue, K. C. Tam, K. Forberich, and C. J. Brabec, "The fabrication of color-tunable organic light-emitting diode displays via solution processing," *Light Sci. Appl.* **6**, e17094 (2017).
- ⁵³C. Keum, C. Murawski, E. Archer, S. Kwon, A. Mischock, and M. C. Gather, "A substrateless, flexible, and water-resistant organic light-emitting diode," *Nat. Commun.* **11**, 6250 (2020).
- ⁵⁴Y. Li, G. Xu, C. Cui, and Y. Li, "Flexible and semitransparent organic solar cells," *Adv. Energy Mater.* **8**, 1701791 (2018).
- ⁵⁵T. M. Clarke and J. R. Durrant, "Charge photogeneration in organic solar cells," *Chem. Rev.* **110**, 6736–6767 (2010).
- ⁵⁶Y. Sun, P. Sheng, C. Di, F. Jiao, W. Xu, D. Qiu, and D. Zhu, "Organic thermoelectric materials and devices based on p- and n-type poly(metal 1,1,2,2-ethenetetrathiolate)s," *Adv. Mater.* **24**, 932–937 (2012).
- ⁵⁷B. Russ, A. Glaudell, J. J. Urban, M. L. Chabinyc, and R. A. Segalman, "Organic thermoelectric materials for energy harvesting and temperature control," *Nat. Rev. Mater.* **1**, 16050 (2016).
- ⁵⁸C.-a. Di, F. Zhang, and D. Zhu, "Multi-functional integration of organic field-effect transistors (OFETs): Advances and perspectives," *Adv. Mater.* **25**, 313–330 (2013).
- ⁵⁹A. Salehi, X. Fu, D.-H. Shin, and F. So, "Recent advances in OLED optical design," *Adv. Funct. Mater.* **29**, 1808803 (2019).
- ⁶⁰Y. Cui, H. Yao, J. Zhang, K. Xian, T. Zhang, L. Hong, Y. Wang, Y. Xu, K. Ma, C. An, C. He, Z. Wei, F. Gao, and J. Hou, "Single-junction organic photovoltaic cells with approaching 18% efficiency," *Adv. Mater.* **32**, 1908205 (2020).
- ⁶¹D. Wang, W. Shi, J. Chen, J. Xi, and Z. Shuai, "Modeling thermoelectric transport in organic materials," *Phys. Chem. Chem. Phys.* **14**, 16505–16520 (2012).
- ⁶²X. Xu, J. Zhou, and J. Chen, "Thermal transport in conductive polymer-based materials," *Adv. Funct. Mater.* **30**, 1904704 (2020).
- ⁶³M. N. Gueye, A. Vercouter, R. Jouclas, D. Guérin, V. Lemaur, G. Schweicher, S. Lenfant, A. Antidormi, Y. Geerts, C. Melis, J. Cornil, and D. Vuillaume, "Thermal conductivity of benzothiopheno-benzothiophene derivatives at the nanoscale," *Nanoscale* **13**, 3800–3807 (2021).
- ⁶⁴X. Y. Wang, J. C. Zhang, Y. Chen, and P. K. L. Chan, "Molecular dynamics study of thermal transport in a dinaphtho 2,3-b;2',3'-f thiено 3,2-b thiophene (DNTT) organic semiconductor," *Nanoscale* **9**, 2262–2271 (2017).
- ⁶⁵M. Mitra, K. Kargupta, S. Ganguly, S. Goswami, and D. Banerjee, "Facile synthesis and thermoelectric properties of aluminum doped zinc oxide/polyaniline (AZO/PANI) hybrid," *Synth. Met.* **228**, 25–31 (2017).
- ⁶⁶W. Kim, "Strategies for engineering phonon transport in thermoelectrics," *J. Mater. Chem. C* **3**, 10336–10348 (2015).
- ⁶⁷D. G. Cahill, S. K. Watson, and R. O. Pohl, "Lower limit to the thermal conductivity of disordered crystals," *Phys. Rev. B* **46**, 6131–6140 (1992).
- ⁶⁸P. B. Allen and J. L. Feldman, "Thermal conductivity of disordered harmonic solids," *Phys. Rev. B* **48**, 12581–12588 (1993).
- ⁶⁹P. B. Allen, J. L. Feldman, J. Fabian, and F. Wooten, "Diffusions, locons and propagons: Character of atomie vibrations in amorphous Si," *Philos. Mag. B* **79**, 1715–1731 (1999).
- ⁷⁰S. Shenogin, A. Bodapati, P. Kebinski, and A. J. H. McGaughey, "Predicting the thermal conductivity of inorganic and polymeric glasses: The role of anharmonicity," *J. Appl. Phys.* **105**, 034906 (2009).
- ⁷¹W. Lv and A. Henry, "Direct calculation of modal contributions to thermal conductivity via Green-Kubo modal analysis," *New J. Phys.* **18**, 013028 (2016).
- ⁷²H. Ushirokita and H. Tada, "In-plane thermal conductivity measurement of conjugated polymer films by membrane-based AC calorimetry," *Chem. Lett.* **45**, 735–737 (2016).
- ⁷³H. Wang, W. Chu, and G. Chen, "A brief review on measuring methods of thermal conductivity of organic and hybrid thermoelectric materials," *Adv. Electron. Mater.* **5**, 1900167 (2019).
- ⁷⁴M. Culebras, B. Uriol, C. M. Gómez, and A. Cantarero, "Controlling the thermoelectric properties of polymers: Application to PEDOT and polypyrrole," *Phys. Chem. Chem. Phys.* **17**, 15140–15145 (2015).
- ⁷⁵G. H. Kim, L. Shao, K. Zhang, and K. P. Pipe, "Engineered doping of organic semiconductors for enhanced thermoelectric efficiency," *Nat. Mater.* **12**, 719–723 (2013).
- ⁷⁶Q. Wei, M. Mukaida, K. Kirihara, and T. Ishida, "Experimental studies on the anisotropic thermoelectric properties of conducting polymer films," *ACS Macro Lett.* **3**, 948–952 (2014).
- ⁷⁷Q. Wei, C. Uehara, M. Mukaida, K. Kirihara, and T. Ishida, "Measurement of in-plane thermal conductivity in polymer films," *AIP Adv.* **6**, 045315 (2016).
- ⁷⁸A. Weathers, Z. U. Khan, R. Brooke, D. Evans, M. T. Pettes, J. W. Andreasen, X. Crispin, and L. Shi, "Significant electronic thermal transport in the conducting polymer poly(3,4-ethylenedioxythiophene)," *Adv. Mater.* **27**, 2101–2106 (2015).

- ⁷⁹V. Linseis, F. Völklein, H. Reith, K. Nielsch, and P. Woias, "Advanced platform for the in-plane ZT measurement of thin films," *Rev. Sci. Instrum.* **89**, 015110 (2018).
- ⁸⁰A. Håkansson, M. Shahi, J. W. Brill, S. Fabiano, and X. Crispin, "Conducting-polymer bolometers for low-cost IR-detection systems," *Adv. Electron. Mater.* **5**, 1800975 (2019).
- ⁸¹H. Park, S. H. Lee, F. S. Kim, H. H. Choi, I. W. Cheong, and J. H. Kim, "Enhanced thermoelectric properties of PEDOT:PSS nanofilms by a chemical dedoping process," *J. Mater. Chem. A* **2**, 6532–6539 (2014).
- ⁸²J. Liu, X. Wang, D. Li, N. E. Coates, R. A. Segelman, and D. G. Cahill, "Thermal conductivity and elastic constants of PEDOT:PSS with high electrical conductivity," *Macromolecules* **48**, 585–591 (2015).
- ⁸³O. Bubnova, Z. U. Khan, A. Malti, S. Braun, M. Fahlman, M. Berggren, and X. Crispin, "Optimization of the thermoelectric figure of merit in the conducting polymer poly(3,4-ethylenedioxythiophene)," *Nat. Mater.* **10**, 429–433 (2011).
- ⁸⁴J. C. Duda, P. E. Hopkins, Y. Shen, and M. C. Gupta, "Thermal transport in organic semiconducting polymers," *Appl. Phys. Lett.* **102**, 251912 (2013).
- ⁸⁵J. A. Malen, K. Baheti, T. Tong, Y. Zhao, J. A. Hudgings, and A. Majumdar, "Optical measurement of thermal conductivity using fiber aligned frequency domain thermoreflectance," *J. Heat. Transfer* **133**, 081601 (2011).
- ⁸⁶S. Kammundur and S. Yee, "A suspended 3-omega technique to measure the anisotropic thermal conductivity of semiconducting polymers," *Rev. Sci. Instrum.* **89**, 114905 (2018).
- ⁸⁷H. Yan, N. Sada, and N. Toshima, "Thermal transporting properties of electrically conductive polyaniline films as organic thermoelectric materials," *J. Therm. Anal. Calorim.* **69**, 881–887 (2002).
- ⁸⁸J. Jin, M. P. Manoharan, Q. Wang, and M. A. Haque, "In-plane thermal conductivity of nanoscale polyaniline thin films," *Appl. Phys. Lett.* **95**, 033113 (2009).
- ⁸⁹J. Wu, Y. Sun, W. Xu, and Q. Zhang, "Investigating thermoelectric properties of doped polyaniline nanowires," *Synthetic Met.* **189**, 177–182 (2014).
- ⁹⁰V. Singh, T. L. Boughez, A. Weathers, Y. Cai, K. Bi, M. T. Pettes, S. A. McMenamin, W. Lv, D. P. Resler, T. R. Gattuso, D. H. Altman, K. H. Sandhage, L. Shi, A. Henry, and B. A. Cola, "High thermal conductivity of chain-oriented amorphous polythiophene," *Nat. Nanotechnol.* **9**, 384–390 (2014).
- ⁹¹J. C. Duda, P. E. Hopkins, Y. Shen, and M. C. Gupta, "Exceptionally low thermal conductivities of films of the fullerene derivative PCBM," *Phys. Rev. Lett.* **110**, 015902 (2013).
- ⁹²X. Wang, C. D. Liman, N. D. Treat, M. L. Chabinyc, and D. G. Cahill, "Ultralow thermal conductivity of fullerene derivatives," *Phys. Rev. B* **88**, 075310 (2013).
- ⁹³J. Wu, Y. Sun, W.-B. Pei, L. Huang, W. Xu, and Q. Zhang, "Polypyrrole nanotube film for flexible thermoelectric application," *Synth. Met.* **196**, 173–177 (2014).
- ⁹⁴B. A. Lunn, J. Unsworth, N. G. Booth, and P. C. Innis, "Determination of the thermal conductivity of polypyrrole over the temperature range 280–335 K," *J. Mater. Sci.* **28**, 5092–5098 (1993).
- ⁹⁵S. Misra, M. Bharti, A. Singh, A. K. Debnath, D. K. Aswal, and Y. Hayakawa, "Nanostructured polypyrrole: Enhancement in thermoelectric figure of merit through suppression of thermal conductivity," *Mater. Res. Express* **4**, 085007 (2017).
- ⁹⁶J. Maiz, M. Muñoz Rojo, B. Abad, A. A. Wilson, A. Nogales, D.-A. Borca-Tasciuc, T. Borca-Tasciuc, and M. Martín-González, "Enhancement of thermoelectric efficiency of doped PCDTBT polymer films," *RSC Adv.* **5**, 66687–66694 (2015).
- ⁹⁷N. Kim, B. Domercq, S. Yoo, A. Christensen, B. Kippelen, and S. Graham, "Thermal transport properties of thin films of small molecule organic semiconductors," *Appl. Phys. Lett.* **87**, 241908 (2005).
- ⁹⁸J. Ràfols-Ribé, R. Dettori, P. Ferrando-Villalba, M. Gonzalez-Silveira, L. Abad, A. F. Lopeandía, L. Colombo, and J. Rodríguez-Viejo, "Evidence of thermal transport anisotropy in stable glasses of vapor deposited organic molecules," *Phys. Rev. Mater.* **2**, 035603 (2018).
- ⁹⁹X. Wang, K. D. Parrish, J. A. Malen, and P. K. L. Chan, "Modifying the thermal conductivity of small molecule organic semiconductor thin films with metal nanoparticles," *Sci. Rep.* **5**, 16095 (2015).
- ¹⁰⁰E. Selezneva, A. Vercouter, G. Schweicher, V. Lemaur, K. Broch, A. Antidormi, K. Takimiya, V. Coropceanu, J.-L. Brédas, C. Melis, J. Cornil, and H. Sirringhaus, "Strong suppression of thermal conductivity in the presence of long terminal alkyl chains in low-disorder molecular semiconductors," *Adv. Mater.* **33**, 2008708 (2021).
- ¹⁰¹D. Trefon-Radziejewska, J. Juszczak, A. Fleming, N. Horny, J. S. Antoniow, M. Chirtoc, A. Kaźmierczak-Bałata, and J. Bodzenta, "Thermal characterization of metal phthalocyanine layers using photothermal radiometry and scanning thermal microscopy methods," *Synth. Met.* **232**, 72–78 (2017).
- ¹⁰²Y. Yao, M. Shahi, M. M. Payne, J. E. Anthony, and J. W. Brill, "Thermal resistances of thin films of small molecule organic semiconductors," *J. Mater. Chem. C* **4**, 8817–8821 (2016).
- ¹⁰³M. Shahi and J. W. Brill, "Frequency-dependent photothermal measurement of thermal diffusivity for opaque and non-opaque materials: Application to crystals of TIPS-pentacene," *J. Appl. Phys.* **124**, 155104 (2018).
- ¹⁰⁴H. Zhang, Y. Yao, M. M. Payne, J. E. Anthony, and J. W. Brill, "Thermal diffusivities of functionalized pentacene semiconductors," *Appl. Phys. Lett.* **105**, 073302 (2014).
- ¹⁰⁵H. Zhang and J. W. Brill, "Interlayer thermal conductivity of rubrene measured by ac-calorimetry," *J. Appl. Phys.* **114**, 043508 (2013).
- ¹⁰⁶Y. Okada, M. Uno, Y. Nakazawa, K. Sasai, K. Matsukawa, M. Yoshimura, Y. Kitaoka, Y. Mori, and J. Takeya, "Low-temperature thermal conductivity of bulk and film-like rubrene single crystals," *Phys. Rev. B* **83**, 113305 (2011).
- ¹⁰⁷M. Sumino, K. Harada, M. Ikeda, S. Tanaka, K. Miyazaki, and C. Adachi, "Thermoelectric properties of n-type C₆₀ thin films and their application in organic thermovoltaic devices," *Appl. Phys. Lett.* **99**, 093308 (2011).
- ¹⁰⁸R. C. Yu, N. Tea, M. B. Salamon, D. Lorrents, and R. Malhotra, "Thermal conductivity of single crystal C₆₀," *Phys. Rev. Lett.* **68**, 2050–2053 (1992).
- ¹⁰⁹P. E. Hopkins, C. M. Reinke, M. F. Su, R. H. Olsson, E. A. Shaner, Z. C. Leseman, J. R. Serrano, L. M. Phinney, and I. El-Kady, "Reduction in the thermal conductivity of single crystalline silicon by phononic crystal patterning," *Nano Lett.* **11**, 107–112 (2011).
- ¹¹⁰M. C. Wingert, Z. C. Y. Chen, E. Dechaumpai, J. Moon, J.-H. Kim, J. Xiang, and R. Chen, "Thermal conductivity of Ge and Ge-Si core-shell nanowires in the phonon confinement regime," *Nano Lett.* **11**, 5507–5513 (2011).
- ¹¹¹J. Kim, S. C. Lee, H. S. Lee, C. W. Kim, and W. H. Lee, "Effects of film microstructure on the bias stability of pentacene field-effect transistors," *Org. Electron.* **29**, 7–12 (2016).
- ¹¹²X. Yu, R. Li, T. Shiga, L. Feng, M. An, L. Zhang, J. Shiomi, and N. Yang, "Hybrid thermal transport characteristics of doped organic semiconductor poly(3,4-ethylenedioxythiophene):tosylate," *J. Phys. Chem. C* **123**, 26735–26741 (2019).
- ¹¹³W. D. Cornell, P. Cieplak, C. I. Bayly, I. R. Gould, K. M. Merz, D. M. Ferguson, D. C. Spellmeyer, T. Fox, J. W. Caldwell, and P. A. Kollman, "A second generation force field for the simulation of proteins, nucleic acids, and organic molecules," *J. Am. Chem. Soc.* **117**, 5179–5197 (1995).
- ¹¹⁴S. J. Weiner, P. A. Kollman, D. A. Case, U. C. Singh, C. Ghio, G. Alagona, S. Profeta, and P. Weiner, "A new force field for molecular mechanical simulation of nucleic acids and proteins," *J. Am. Chem. Soc.* **106**, 765–784 (1984).
- ¹¹⁵S. J. Weiner, P. A. Kollman, D. T. Nguyen, and D. A. Case, "An all atom force field for simulations of proteins and nucleic acids," *J. Comput. Chem.* **7**, 230–252 (1986).
- ¹¹⁶W. L. Jorgensen, D. S. Maxwell, and J. Tirado-Rives, "Development and testing of the OPLS all-atom force field on conformational energetics and properties of organic liquids," *J. Am. Chem. Soc.* **118**, 11225–11236 (1996).
- ¹¹⁷W. L. Jorgensen and J. Tirado-Rives, "The OPLS [optimized potentials for liquid simulations] potential functions for proteins, energy minimizations for crystals of cyclic peptides and crambin," *J. Am. Chem. Soc.* **110**, 1657–1666 (1988).
- ¹¹⁸A. D. MacKerell, D. Bashford, M. Bellott, R. L. Dunbrack, J. D. Evanseck, M. J. Field, S. Fischer, J. Gao, H. Guo, S. Ha, D. Joseph-McCarthy, L. Kuchnir,

- K. Kuczera, F. T. K. Lau, C. Mattos, S. Michnick, T. Ngo, D. T. Nguyen, B. Prodhom, W. E. Reiher, B. Roux, M. Schlenkrich, J. C. Smith, R. Stote, J. Straub, M. Watanabe, J. Wiorkiewicz-Kuczera, D. Yin, and M. Karplus, "All-atom empirical potential for molecular modeling and dynamics studies of proteins," *J. Phys. Chem. B* **102**, 3586–3616 (1998).
- ¹¹⁹A. D. MacKerell, J. Wiorkiewicz-Kuczera, and M. Karplus, "An all-atom empirical energy function for the simulation of nucleic acids," *J. Am. Chem. Soc.* **117**, 11946–11975 (1995).
- ¹²⁰B. R. Brooks, R. E. Bruccoleri, B. D. Olafson, D. J. States, S. Swaminathan, and M. Karplus, "CHARMM: A program for macromolecular energy, minimization, and dynamics calculations," *J. Comput. Chem.* **4**, 187–217 (1983).
- ¹²¹P. Dauber-Osguthorpe, V. A. Roberts, D. J. Osguthorpe, J. Wolff, M. Genest, and A. T. Hagler, "Structure and energetics of ligand binding to proteins: *Escherichia coli* dihydrofolate reductase-trimethoprim, a drug-receptor system," *Proteins* **4**, 31–47 (1988).
- ¹²²J. Wang, R. M. Wolf, J. W. Caldwell, P. A. Kollman, and D. A. Case, "Development and testing of a general amber force field," *J. Comput. Chem.* **25**, 1157–1174 (2004).
- ¹²³H. Sun, "Force field for computation of conformational energies, structures, and vibrational frequencies of aromatic polyesters," *J. Comput. Chem.* **15**, 752–768 (1994).
- ¹²⁴H. Sun, S. J. Mumby, J. R. Maple, and A. T. Hagler, "Ab initio calculations on small molecule analogs of polycarbonates," *J. Phys. Chem.* **99**, 5873–5882 (1995).
- ¹²⁵H. Sun, "COMPASS: An ab initio force-field optimized for condensed-phase applications—Overview with details on alkane and benzene compounds," *J. Phys. Chem. B* **102**, 7338–7364 (1998).
- ¹²⁶H. Sun, P. Ren, and J. R. Fried, "The COMPASS force field: Parameterization and validation for phosphazenes," *Comput. Theor. Polym. Sci.* **8**, 229–246 (1998).
- ¹²⁷D. Wang, L. Tang, M. Q. Long, and Z. G. Shuai, "Anisotropic thermal transport in organic molecular crystals from nonequilibrium molecular dynamics simulations," *J. Phys. Chem. C* **115**, 5940–5946 (2011).
- ¹²⁸W. Shi, Z. Shuai, and D. Wang, "Tuning thermal transport in chain-oriented conducting polymers for enhanced thermoelectric efficiency: A computational study," *Adv. Funct. Mater.* **27**, 1702847 (2017).
- ¹²⁹C. Shao, Y. Jin, K. Pipe, M. Shtein, and J. Kieffer, "Simulation of crystalline and amorphous copper phthalocyanine: Force field development and analysis of thermal transport mechanisms," *J. Phys. Chem. C* **118**, 9861–9870 (2014).
- ¹³⁰S. Wu, Y. Kondo, M.-a. Kakimoto, B. Yang, H. Yamada, I. Kuwajima, G. Lambard, K. Hongo, Y. Xu, J. Shiomi, C. Schick, J. Morikawa, and R. Yoshida, "Machine-learning-assisted discovery of polymers with high thermal conductivity using a molecular design algorithm," *NPJ Comput. Mater.* **5**, 66 (2019).
- ¹³¹X. Qian, S. Peng, X. Li, Y. Wei, and R. Yang, "Thermal conductivity modeling using machine learning potentials: Application to crystalline and amorphous silicon," *Mater. Today Phys.* **10**, 100140 (2019).
- ¹³²P. Korotaev, I. Novoselov, A. Yanilkin, and A. Shapeev, "Accessing thermal conductivity of complex compounds by machine learning interatomic potentials," *Phys. Rev. B* **100**, 144308 (2019).
- ¹³³B. Mortazavi, E. V. Podryabinkin, S. Roche, T. Rabczuk, X. Zhuang, and A. V. Shapeev, "Machine-learning interatomic potentials enable first-principles multiscale modeling of lattice thermal conductivity in graphene/borophene heterostructures," *Mater. Horiz.* **7**, 2359–2367 (2020).
- ¹³⁴S. Maeno, J. J. Cannon, T. Shiga, and J. Shiomi, "Molecular dynamics study on heat conduction in poly(3,4-ethylenedioxythiophene)," *Jpn. J. Appl. Phys.* **57**, 101601 (2018).
- ¹³⁵M. G. Holland, "Analysis of lattice thermal conductivity," *Phys. Rev.* **132**, 2461–2471 (1963).
- ¹³⁶C. Lin, X. Chen, and X. Zou, "Phonon-grain-boundary-interaction-mediated thermal transport in two-dimensional polycrystalline MoS₂," *ACS Appl. Mater. Interfaces* **11**, 25547–25555 (2019).
- ¹³⁷S. Qu, Q. Yao, L. Wang, Z. Chen, K. Xu, H. Zeng, W. Shi, T. Zhang, C. Uher, and L. Chen, "Highly anisotropic P3HT films with enhanced thermoelectric performance via organic small molecule epitaxy," *NPJ Asia Mater.* **8**, e292 (2016).
- ¹³⁸J. Liu, Y. Sun, X. Gao, R. Xing, L. Zheng, S. Wu, Y. Geng, and Y. Han, "Oriented poly(3-hexylthiophene) nanofibril with the π-π stacking growth direction by solvent directional evaporation," *Langmuir* **27**, 4212–4219 (2011).
- ¹³⁹V. Skrypnichuk, N. Boulanger, V. Yu, M. Hilke, S. C. B. Mannsfeld, M. F. Toney, and D. R. Barbero, "Enhanced vertical charge transport in a semiconducting P3HT thin film on single layer graphene," *Adv. Funct. Mater.* **25**, 664–670 (2015).
- ¹⁴⁰T. Zhou, Z. H. Li, Y. J. Cheng, Y. X. Ni, S. Volz, D. Donadio, S. Y. Xiong, W. Q. Zhang, and X. H. Zhang, "Thermal transport in amorphous small organic materials: A mechanistic study," *Phys. Chem. Chem. Phys.* **22**, 3058–3065 (2020).
- ¹⁴¹Y. Xu, X. Wang, J. Zhou, B. Song, Z. Jiang, E. M. Y. Lee, S. Huberman, K. K. Gleason, and G. Chen, "Molecular engineered conjugated polymer with high thermal conductivity," *Sci. Adv.* **4**, eaar3031 (2018).
- ¹⁴²R. Sarabia-Riquelme, M. Shahi, J. W. Brill, and M. C. Weisenberger, "Effect of drawing on the electrical, thermoelectrical, and mechanical properties of wet-spun PEDOT:PSS fibers," *ACS Appl. Polym. Mater.* **1**, 2157–2167 (2019).
- ¹⁴³M. K. Smith, V. Singh, K. Kalaitzidou, and B. A. Cola, "Poly(3-hexylthiophene) nanotube array surfaces with tunable wetting and contact thermal energy transport," *ACS Nano* **9**, 1080–1088 (2015).
- ¹⁴⁴W. Shi, J. M. Chen, J. Y. Xi, D. Wang, and Z. G. Shuai, "Search for organic thermoelectric materials with high mobility: The case of 2,7-dialkyl[1]benzothieno[3,2-b][1]benzothiophene derivatives," *Chem. Mater.* **26**, 2669–2677 (2014).
- ¹⁴⁵H. Zheng, K. Wu, W. Chen, B. Nan, Z. Qu, and M. Lu, "High intrinsic thermal conductivity of polythiophene by reducing steric hindrance and enhancing p-π conjugation," *Macromol. Chem. Phys.* **222**, 2000418 (2021).
- ¹⁴⁶Y. Wang, C. Yang, Y.-W. Mai, and Y. Zhang, "Effect of non-covalent functionalisation on thermal and mechanical properties of graphene-polymer nanocomposites," *Carbon* **102**, 311–318 (2016).
- ¹⁴⁷J. Lu, K. Yuan, F. Sun, K. Zheng, Z. Zhang, J. Zhu, X. Wang, X. Zhang, Y. Zhuang, Y. Ma, X. Cao, J. Zhang, and D. Tang, "Self-assembled monolayers for the polymer/semiconductor interface with improved interfacial thermal management," *ACS Appl. Mater. Interfaces* **11**, 42708–42714 (2019).
- ¹⁴⁸S. Kuang and J. D. Gezelter, "Simulating interfacial thermal conductance at metal-solvent interfaces: The role of chemical capping agents," *J. Phys. Chem. C* **115**, 22475–22483 (2011).
- ¹⁴⁹L. Hu, T. Desai, and P. Kebinski, "Thermal transport in graphene-based nanocomposite," *J. Appl. Phys.* **110**, 033517 (2011).
- ¹⁵⁰R. S. Prasher and P. E. Phelan, "A scattering-mediated acoustic mismatch model for the prediction of thermal boundary resistance," *J. Heat Transfer* **123**, 105–112 (2001).
- ¹⁵¹P. E. Hopkins and P. M. Norris, "Effects of joint vibrational states on thermal boundary conductance," *Nanosc. Microsc. Therm.* **11**, 247–257 (2007).
- ¹⁵²P. E. Hopkins, "Multiple phonon processes contributing to inelastic scattering during thermal boundary conductance at solid interfaces," *J. Appl. Phys.* **106**, 013528 (2009).
- ¹⁵³J. Park, W. H. Lee, S. Huh, S. H. Sim, S. B. Kim, K. Cho, B. H. Hong, and K. S. Kim, "Work-function engineering of graphene electrodes by self-assembled monolayers for high-performance organic field-effect transistors," *J. Phys. Chem. Lett.* **2**, 841–845 (2011).
- ¹⁵⁴X. Wang, L. Zhi, and K. Müllen, "Transparent, conductive graphene electrodes for dye-sensitized solar cells," *Nano Lett.* **8**, 323–327 (2008).
- ¹⁵⁵X. Wang, H. Fan, D. Han, Y. Hong, and J. Zhang, "Thermal boundary resistance at graphene-pentacene interface explored by a data-intensive approach," *Nanotechnology* **32**, 215404 (2021).
- ¹⁵⁶X. Wang, J. Zhang, Y. Chen, and P. K. L. Chan, "Investigation of interfacial thermal transport across graphene and an organic semiconductor using molecular dynamics simulations," *Phys. Chem. Chem. Phys.* **19**, 15933–15941 (2017).

- ¹⁵⁷H. Ma, H. Babaei, and Z. Tian, "The importance of van der Waals interactions to thermal transport in graphene-C₆₀ heterostructures," *Carbon* **148**, 196–203 (2019).
- ¹⁵⁸Z.-S. Wu, G. Zhou, L.-C. Yin, W. Ren, F. Li, and H.-M. Cheng, "Graphene/metal oxide composite electrode materials for energy storage," *Nano Energy* **1**, 107–131 (2012).
- ¹⁵⁹J. Hu, X. Ruan, and Y. P. Chen, "Thermal conductivity and thermal rectification in graphene nanoribbons: A molecular dynamics study," *Nano Lett.* **9**, 2730–2735 (2009).
- ¹⁶⁰Z. Zhang, G. Chen, H. Wang, and X. Li, "Template-directed *in situ* polymerization preparation of nanocomposites of PEDOT:PSS-coated multi-walled carbon nanotubes with enhanced thermoelectric property," *Chem. Asian J.* **10**, 149–153 (2015).
- ¹⁶¹D. L. Niko, A. S. Askerov, and A. A. Balandin, "Anomalous size dependence of the thermal conductivity of graphene ribbons," *Nano Lett.* **12**, 3238–3244 (2012).
- ¹⁶²B. Liu, J. A. Baimova, C. D. Reddy, A. W.-K. Law, S. V. Dmitriev, H. Wu, and K. Zhou, "Interfacial thermal conductance of a silicene/graphene bilayer heterostructure and the effect of hydrogenation," *ACS Appl. Mater. Interfaces* **6**, 18180–18188 (2014).
- ¹⁶³J. Zhang, Y. Hong, and Y. Yue, "Thermal transport across graphene and single layer hexagonal boron nitride," *J. Appl. Phys.* **117**, 134307 (2015).
- ¹⁶⁴I. Kröger, B. Stadtmüller, C. Stadler, J. Ziroff, M. Kochler, A. Stahl, F. Pollinger, T.-L. Lee, J. Zegenhagen, F. Reinert, and C. Kumpf, "Submonolayer growth of copper-phthalocyanine on Ag(111)," *New J. Phys.* **12**, 083038 (2010).
- ¹⁶⁵C. Stadler, S. Hansen, I. Kröger, C. Kumpf, and E. Umbach, "Tuning intermolecular interaction in long-range-ordered submonolayer organic films," *Nat. Phys.* **5**, 153–158 (2009).
- ¹⁶⁶B. Stadtmüller, I. Kröger, F. Reinert, and C. Kumpf, "Submonolayer growth of CuPc on noble metal surfaces," *Phys. Rev. B* **83**, 085416 (2011).
- ¹⁶⁷Y. Jin, C. Shao, J. Kieffer, M. L. Falk, and M. Shtein, "Spatial nonuniformity in heat transport across hybrid material interfaces," *Phys. Rev. B* **90**, 054306 (2014).
- ¹⁶⁸D. Prashar, "Self assembled monolayers—A review," *Int. J. Chemtech Res.* **4**, 258–265 (2012).
- ¹⁶⁹B.-H. Huisman, R. P. H. Kooyman, F. C. J. M. van Veggel, and D. N. Reinhoudt, "Molecular recognition by self-assembled monolayers detected with surface plasmon resonance," *Adv. Mater.* **8**, 561–564 (1996).
- ¹⁷⁰K. D. Schierbaum, T. Weiss, E. U. T. van Veizen, J. F. J. Engbersen, D. N. Reinhoudt, and W. Göpel, "Molecular recognition by self-assembled monolayers of cavitand receptors," *Science* **265**, 1413 (1994).
- ¹⁷¹Y.-S. Shon, S. Lee, R. Colorado, S. S. Perry, and T. R. Lee, "Spiroalkanedithiol-based SAMs reveal unique insight into the wettabilities and frictional properties of organic thin films," *J. Am. Chem. Soc.* **122**, 7556–7563 (2000).
- ¹⁷²D. J. Diaz, J. E. Hudson, G. D. Storrier, H. D. Abruna, N. Sundararajan, and C. K. Ober, "Lithographic applications of redox probe microscopy," *Langmuir* **17**, 5932–5938 (2001).
- ¹⁷³A. Carvalho, M. Geissler, H. Schmid, B. Michel, and E. Delamarche, "Self-assembled monolayers of eicosanethiol on palladium and their use in microcontact printing," *Langmuir* **18**, 2406–2412 (2002).
- ¹⁷⁴X. Wei, T. Zhang, and T. Luo, "Thermal energy transport across hard-soft interfaces," *ACS Energy Lett.* **2**, 2283–2292 (2017).
- ¹⁷⁵L. Zhang, Z. Bai, and L. Liu, "Exceptional thermal conductance across hydrogen-bonded graphene/polymer interfaces," *Adv. Mater. Interfaces* **3**, 1600211 (2016).
- ¹⁷⁶Y. Xiong, X. Yu, Y. Huang, J. Yang, L. Li, N. Yang, and D. Xu, "Ultralow thermal conductance of the van der Waals interface between organic nanoribbons," *Mater. Today Phys.* **11**, 100139 (2019).
- ¹⁷⁷L.-D. Zhao, S.-H. Lo, Y. Zhang, H. Sun, G. Tan, C. Uher, C. Wolverton, V. P. Dravid, and M. G. Kanatzidis, "Ultralow thermal conductivity and high thermoelectric figure of merit in SnSe crystals," *Nature* **508**, 373–377 (2014).
- ¹⁷⁸G. K. H. Madsen, "Automated search for new thermoelectric materials: The case of LiZnSb," *J. Am. Chem. Soc.* **128**, 12140–12146 (2006).
- ¹⁷⁹G. D. Mahan and J. O. Sofo, "The best thermoelectric," *Proc. Natl. Acad. Sci. U.S.A.* **93**, 7436 (1996).
- ¹⁸⁰J. Yang, H. Li, T. Wu, W. Zhang, L. Chen, and J. Yang, "Evaluation of half-Heusler compounds as thermoelectric materials based on the calculated electrical transport properties," *Adv. Funct. Mater.* **18**, 2880–2888 (2008).
- ¹⁸¹X. Shi, J. Yang, J. R. Salvador, M. Chi, J. Y. Cho, H. Wang, S. Bai, J. Yang, W. Zhang, and L. Chen, "Multiple-filled skutterudites: High thermoelectric figure of merit through separately optimizing electrical and thermal transports," *J. Am. Chem. Soc.* **133**, 7837–7846 (2011).
- ¹⁸²W. Shi, T. Zhao, J. Xi, D. Wang, and Z. Shuai, "Unravelling doping effects on PEDOT at the molecular level: From geometry to thermoelectric transport properties," *J. Am. Chem. Soc.* **137**, 12929–12938 (2015).
- ¹⁸³X. Yong, W. Shi, G. Wu, S. S. Goh, S. Bai, J.-W. Xu, J.-S. Wang, and S.-W. Yang, "Tuning the thermoelectric performance of π-d conjugated nickel coordination polymers through metal-ligand frontier molecular orbital alignment," *J. Mater. Chem. A* **6**, 19757–19766 (2018).
- ¹⁸⁴J. Khan, Y. Liu, T. Zhao, H. Geng, W. Xu, and Z. Shuai, "High performance thermoelectric materials based on metal organic coordination polymers through first-principles band engineering," *J. Comput. Chem.* **39**, 2582–2588 (2018).
- ¹⁸⁵T. Zhao, W. Shi, J. Xi, D. Wang, and Z. Shuai, "Intrinsic and extrinsic charge transport in CH₃NH₃PbI₃ perovskites predicted from first-principles," *Sci. Rep.* **6**, 19968 (2016).
- ¹⁸⁶D. Wang, L. Tang, M. Long, and Z. Shuai, "First-principles investigation of organic semiconductors for thermoelectric applications," *J. Chem. Phys.* **131**, 224704 (2009).
- ¹⁸⁷J. Chen, D. Wang, and Z. Shuai, "First-principles predictions of thermoelectric figure of merit for organic materials: Deformation potential approximation," *J. Chem. Theory Comput.* **8**, 3338–3347 (2012).
- ¹⁸⁸W. Shi, D. Wang, and Z. Shuai, "High-performance organic thermoelectric materials: Theoretical insights and computational design," *Adv. Electron. Mater.* **5**, 1800882 (2019).
- ¹⁸⁹L. Groenendaal, F. Jonas, D. Freitag, H. Pielartzik, and J. R. Reynolds, "Poly(3,4-ethylenedioxythiophene) and its derivatives: Past, present, and future," *Adv. Mater.* **12**, 481–494 (2000).
- ¹⁹⁰D. A. Mengistie, C.-H. Chen, K. M. Boopathi, F. W. Pranoto, L.-J. Li, and C.-W. Chu, "Enhanced thermoelectric performance of PEDOT:PSS flexible bulky papers by treatment with secondary dopants," *ACS Appl. Mater. Interfaces* **7**, 94–100 (2015).
- ¹⁹¹D. Yuan, L. Liu, X. Jiao, Y. Zou, C. R. McNeill, W. Xu, X. Zhu, and D. Zhu, "Quinoid-resonant conducting polymers achieve high electrical conductivity over 4000 S cm⁻¹ for thermoelectrics," *Adv. Sci.* **5**, 1800947 (2018).
- ¹⁹²Y. Sun, L. Qiu, L. Tang, H. Geng, H. Wang, F. Zhang, D. Huang, W. Xu, P. Yue, Y.-s. Guan, F. Jiao, Y. Sun, D. Tang, C.-a. Di, Y. Yi, and D. Zhu, "Flexible n-type high-performance thermoelectric thin films of poly(nickel-ethylenetetrathiolate) prepared by an electrochemical method," *Adv. Mater.* **28**, 3351–3358 (2016).
- ¹⁹³H. Kojima, R. Abe, F. Fujiwara, M. Nakagawa, K. Takahashi, D. Kuzuhara, H. Yamada, Y. Yakiyama, H. Sakurai, T. Yamamoto, H. Yakushiji, M. Ikeda, and M. Nakamura, "Universality of the giant Seebeck effect in organic small molecules," *Mater. Chem. Front.* **2**, 1276–1283 (2018).
- ¹⁹⁴C. Cho, K. L. Wallace, P. Tzeng, J.-H. Hsu, C. Yu, and J. C. Grunlan, "Outstanding low temperature thermoelectric power factor from completely organic thin films enabled by multidimensional conjugated nanomaterials," *Adv. Energy Mater.* **6**, 1502168 (2016).
- ¹⁹⁵P.-A. Zong, P. Zhang, S. Yin, Y. Huang, Y. Wang, and C. Wan, "Fabrication and characterization of a hybrid Bi₂Se₃/organic superlattice for thermoelectric energy conversion," *Adv. Electron. Mater.* **5**, 1800842 (2019).